Analysis of war and conflict effect on the transmission dynamics of the tenth Ebola outbreak in the Democratic Republic of Congo

Michael Chapwanya[1,*], Jean Lubuma[2], Yibeltal Terefe[3] and Berge Tsanou[1,4]

[1]Department of Mathematics & Applied Mathematics, University of Pretoria, Pretoria, South Africa

[2]School of Computer Science & Applied Mathematics, University of the Witwatersrand, Johannesburg, South A

[3]Department of Mathematics & Applied Mathematics, University of the Free State, Bloemfontein, South Afr

[4]Department of Mathematics & Computer Sciences, University of Dschang, Dschang, Cameroon

Abstract

The tenth Ebola outbreak in the Democratic Republic of Congo (DRC) that occurred from 2018-2020 was exacerbated by long-lasting conflicts and war in the region. We propose a deterministic model to investigate the impact of such disruptive events on the transmission dynamics of the Ebola Virus Disease (EVD). It is an extension of the classical Susceptible-Infectious-Recovered (SIR) model, enriched by an additional class of contaminated environment to account for indirect transmission as well as two classes of hospitalized individuals and patients who escape from the healthcare facility due to violence and attacks perpetrated by armed groups, rebels, *etc.* The model is formulated using two patches, namely Patch 1 consisting of the three affected eastern provinces in DRC and Patch 2, a war- and conflict-free area consisting of the go-to neighbouring provinces for escaped patients. We introduce two key parameters, the escaping rate from hospitals and the destruction of hospitals, in terms of which the effect of war and conflicts is measured. The model is fitted and parametrized using the cumulative mortality data from the region. The basic reproduction number $\mathcal{R}_0$ is computed and found to have a complex expression due to the high nonlinearity of the model. By using, not a Lyapunov function, but a decomposition theorem in Castillo-Chavez et al. (2002), it is shown that the disease-free equilibrium is globally asymptotically stable when $\mathcal{R}_0 < 1$ and unstable when $\mathcal{R}_0 > 1$. A nonstandard finite difference scheme which replicates the dynamics of the continuous model is designed. In particular, a discrete counterpart of the above-mentioned theorem on the global asymptotic stability of the disease-free equilibrium is investigated. Numerical experiments are presented to support the theoretical results.

*Corresponding author. m.chapwanya@up.ac.za; Tel.: +27 12 420 2837; Fax.: +27 12 420 3893

When $\mathcal{R}_0 > 1$, the numerical simulations suggest that there exists for the full model a unique globally asymptotically stable interior endemic equilibrium point, while it is shown theoretically and computationally that the model possesses at least a one Patch 1 and a one Patch 2 boundary equilibria (*i.e.,* Patch 2 and Patch 1 disease-free equilibrium) points, which are locally asymptotically stable. Some recommendations to tackle Ebola in a conflict zone are stated.

Keywords: Ebola Virus Disease, conflict dynamics, Patch model, Basic reproduction number, Stability, Nonstandard finite difference method

AMS Subject Classification: $34A34$, $37N25$, $65L12$, $65L99$, $92B05$, $92D30$

1 Introduction

Ebola Virus Disease (EVD), formerly known as Ebola Haemorrhagic Fever (EHF), was first identified in 1976 with two simultaneous outbreaks in Sudan and Zaire, now the Democratic Republic of Congo (DRC) (WHO 2014). The latter occurred in the village of Yambuku near the Ebola River, from which the disease takes its name. Since then, there has been a recurrence of 29 outbreaks in the tropical regions of the Sub-Saharan Africa (CDC 2021). The DRC alone counts for more than 10 outbreaks, and in this work, we will come back often to this country.

EVD is a major public health disaster and threat to both Sub-Saharan Africa countries with wide-spread transmission and other countries in the world affected during the epidemic. This is to the extent that, on two occasions (*i.e.* 8 August 2014 and 17 July 2019) in a relatively short period of time, the World Health Organization (WHO) declared a Public Health Emergency of International Concern (PHEIC) for the Ebola virus disease outbreaks in West Africa (2014-2016) and in DRC (2018-2020), respectively (WHO 2019*a*, CDC 2019). The impact these largest Ebola outbreaks had on the world, and particularly West Africa, is significant. A total of 28,616 cases of EVD and 11,310 deaths were reported in Guinea, Liberia, and Sierra Leone. There were an additional 36 cases and 15 deaths that occurred when the outbreak spread outside of these three countries (CDC 2019). The DRC recorded 3481 cases and 2299 deaths (WHO 2020*a*).

The recurrence of Ebola outbreaks is a cause for concern. A number of studies have been undertaken to this effect. For instance, the work (Berge et al. 2017c) addresses the following research question, which paved the way to indirect transmission: 'can the consumption of contaminated bush meat, the funeral practices, and the environmental contamination explain the recurrence and persistence of EVD outbreaks in Africa?' Naturally, the authors coupled the question with the well-known direct transmission route, which involves contact with: (1) blood or body fluid (including but not limited to urine, saliva, sweat, feces, vomit, breast milk, and semen); (2) objects (e.g. clothes, bedding) that have been contaminated with body fluid.

While the traditional beliefs and customs of Africans can be a source of problems (Agusto et al. 2015), there are fundamental challenges that have contributed to the prolonged repetition

of EVD outbreaks and unsuccessful fight against the epidemic. The findings in the paper (Buseh et al. 2015) are critical in several respects including the two main ones below. Firstly, 'the Ebola epidemic in West Africa has drawn attention to global health inequalities, in particular, the inadequacies of health care systems in sub-Saharan African countries for appropriately managing and containing infectious diseases.' Secondly, 'there exist sociopolitical and economic conditions that created the environment for the Ebola epidemic to occur'. In this regard, it is important to note that 'structurally, all the countries that were at the epicenter of Ebola in West Africa emerged from civil conflicts with dysfunctional and fragile health systems.' These findings are echoed in the articles (Kraemer et al. 2020, Maxmen 2019, Wells et al. 2019) that are devoted to the 2018-2020 EVD in DRC.

Actually, what happened during the latter outbreak better demonstrates that conflicts and political events precede the surge of Ebola cases. The eastern region of DRC has been confronting chronic conflict and war for money and power gains. In this region, the presidential and general elections were suspended in December 2018. Protesters angry with the postponement burnt tires and ransacked on the Ebola Treatment Center (ETC) in Beni on 27 December 2018, causing 21 (suspected and confirmed) patients to flee (BBC News 2018, Wells et al. 2019). More generally, the instability created by this political decision forced one million people to be displaced in the region and to embrace cramped living conditions that are conducive to the transmission of Ebola and to increases in numbers of cases (Tumutegyereize 2019). Indeed, as stated in the comparative study (McPake et al. 2015) concerning Northern Uganda (sharing a border with DRC) and Sierra Leone (in West Africa), 'those whose normal subsistence is undermined, for example, because their homestead is made insecure and those who are active conflict participants, appear to be at increased risk of being infected.' From the same reference (McPake et al. 2015), it is concluded that 'conflict and its aftermath are among the factors that increase the opportunity for Ebola virus to transmit from a forest animal to a human by disrupting livelihoods and living arrangements.'

The 2018-2020 EVD in DRC was the first outbreak to occur in a tumultuous eastern region; it was the first one in an active conflict and war zone (Maxmen 2019, Tumutegyereize 2019). Unprecedented challenges were associated with this outbreak. These included:

- *The spread of the disease in areas with cross-border population flow.* For instance, the Ugandan Ministry of Health and WHO confirmed three and one cross-border cases on 11 June 2019 and 29 August 2019, respectively (Médecins Sans Frontières 2021*a*).

- *The repeated attacks of Ebola Treatment Centers (ETCs), and escape of patients from the hospitals.* In North Kivu and Ituri provinces, violence was perpetuated by more than 100 armed groups who were fighting for resources. A total number of 174 healthcare workers were attacked in 2019 (Tumutegyereize 2019). On 24 February 2019, ETCs were burnt in Katwa and Butembo; healthcare workers staff were evacuated, while four patients fled into the forest (Maxmen 2019, Wells et al. 2019).

Region/ Country of outbreak	**Outbreak period**	**Hospital beds (Physicians) *per* 1000 people**	**Total cases**	**Total deaths**
Active conflict Eastern DRC	2018-2020	0.8 (0.1)	**3481**	**2299**
Pre-conflict West Africa				
Guinea	2014-2016	0.3 (0.1)	3814	2544
Liberia	2014-2016	0.8 (0.0)	10678	4810
Sierra Leone	2014-2016	0.4 (0.0)	14124	3956
Subtotal cases and deaths			**28616**	**11310**
Widespread transmission				
Italy	2014-2016	3.1 (4)	1	0
Mali	2014-2016	0.1 (0.1)	8	6
Nigeria	2014-2016	0.5 (0.4)	20	8
Senegal	2014-2016	0.3 (0.1)	1	0
Spain	2014-2016	3 (3.9)	1	0
Uganda	2018-2020	0.5 (0.2)	4	4
United Kingdom	2014-2016	2.5 (2.8)	1	0
United States	2014-2016	2.9 (2.6)	4	1
Subtotal cases and deaths			**40**	**19**
Total cases and deaths	2014-2016		**28652**	**11325**
	2018-2020		**3485**	**2303**

Table 1: The largest and severe Ebola outbreaks in the context of conflict affected regions

- *The lack of access to affected communities by healthcare workers* (Kasereka et al. 2019, Maxmen 2018).

- *The increase in numbers of cases among healthcare workers e.g. 5% (168 cases) of the total confirmed cases on 31 December 2019* (WHO 2020*b*).

- *The increase in numbers of cases and affected areas.* It is seen from the map (right) in Figure 1 that the 2018-2020 Ebola outbreak was observed first in August 2018 in Mabalako (yellow) before spreading in several areas (brown) in North Kivu, South Kivu and Ituri provinces. The map also provides information on study location (purple) and other Ebola virus outbreaks (orange) in the DRC to date (Goldstein et al. 2020). The following additional observations are of great importance in our study. Together, the three affected provinces counted about 23 million inhabitants and occupied 74 thousand square kilometers, which represented 25% and 3% of the corresponding figures of the DRC (left map) (DRC Ministry 2021). Hence the population density *per* square kilometer is 310 for the region versus 38.2 for the whole country (World Bank 2019*c*). This discrepancy is in contrast with the fact that there were only 11 Ebola Treatment Centres and 25 Ebola Transit Centres across the region; see External Situation Report 78 (2019) (WHO 2019*b*).

This explains in the map (right) the location of the villages and the Rubare Health Center in Rutshuru Health Zone in North Kivu province where febrile study participants traveled from and were treated prior to Ebola Virus Disease outbreak in Eastern DRC that began in 2018 (Goldstein et al. 2020).

- *The war zone complicating the roll-out of Ebola vaccine, and other control and management strategies such as isolation and contact tracing* (Maxmen 2019, Wells et al. 2019).

For a quick reflection on the impact of conflict and war, we have included Table 1 that displays some information on countries affected by the EVD. Most of the statistics is taken from (World Bank 2019*b*, 2017, CDC 2019). With the respective numbers of hospital beds and physicians *per* 1,000 people varying between 0.1-0.8 and 0.0-0.4 (Africa) versus 2.5-3.1 and 2.6-4 (Europe and US), the table illustrates that healthcare systems in sub-Saharan African countries are comparatively very weak. Adding to this the fact that healthcare facilities were often attacked and destroyed, (Kraemer et al. 2020, Maxmen 2019, Wells et al. 2019, Tumutegyereize 2019), makes it challenging to control and manage the spread of the EVD. That Liberia and Sierra Leone have 0.0 physicians *per* 1,000 people accounts for the civil wars that brought all the health systems down in these countries (Kruk et al. 2010, Omondi & Sheriff 2010).

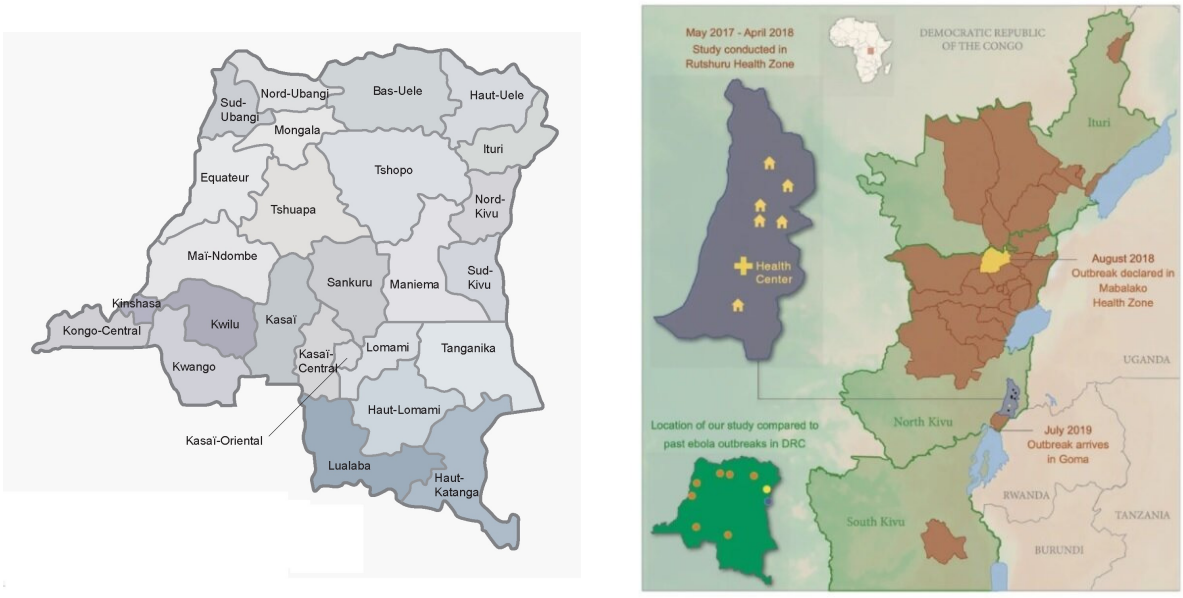

Figure 1: DRC provinces map (left) and 2018-2020 EVD distribution map (Goldstein et al. 2020) (right)

Last but not least! It is instructive to look at Table 1 and Figure 1 in conjunction with Figure 2 extracted from the annual report of the DRC Ministry of Health (DRC Ministry 2021). This figure illustrates that the highest number of cases (2842), deaths (1783) and fatality rate (62.74%) occurred in the year 2019 when the conflict/war in the region was at its peak. **Note that there were no Ebola outbreaks in 2016, which is a zero by zero situation as**

indicated in the figure. On the contrary, a short Ebola outbreak arose in 2017, with 8 reported cases out of which 3 died (which corresponds to a fatality of about 38% as indicated in Figure 2); see External Situation Report 22 (WHO 2017).

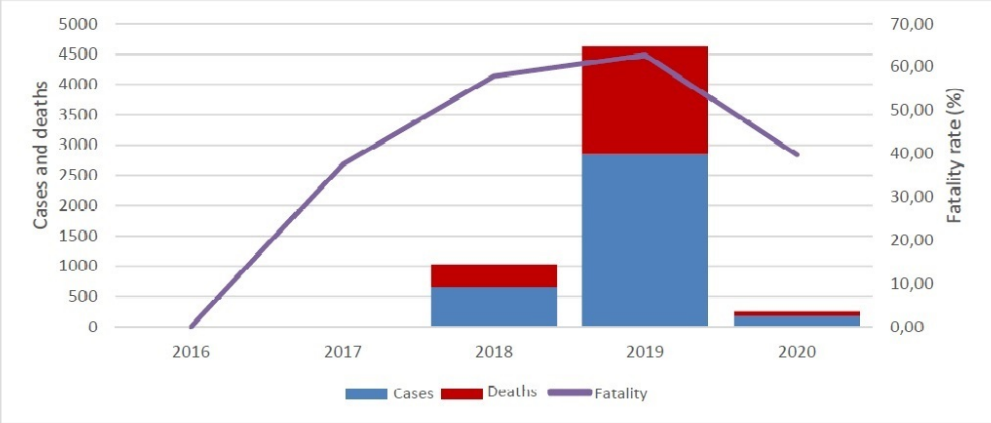

Figure 2: Evolution of cases, deaths and fatality rate for EVD in DRC from 2016 to 2020 (DRC Ministry 2021)

The purpose of this work is to study the impact of conflict and war on the transmission dynamics, and the control and eradication of the Ebola virus disease. Given that the North-Eastern of the Democratic Republic of the Congo is in a chronic state of conflict and experiences, till now, EVD outbreaks (the latest was declared in North Kivu on 7 February 2021 (Médecins Sans Frontières 2021*c*)), the study will mostly focus on the 2018-2020 epidemic, which, as mentioned earlier, is the largest ever recorded in DRC and the first of its kind to happen in the tumultuous and active conflict provinces of North Kivu and Ituri (See the maps in Figure 1).

Though the research question under consideration is highly relevant, there is limited understanding of what ramifications conflict events have on disease transmission and control in region plagued by civil unrest, violence and war (Wells et al. 2019). Here is an indication on a couple of investigations that have been carried out to this effect.

The authors in (Kraemer et al. 2020) characterized the association between variables documenting broad conflict levels and EVD transmission. It was observed that the incidence of conflict *per capita* was correlated with the incidence of EVD *per capita* at the health zone level only for the entire outbreak (Pearson's $\rho = 0.33$, 95% CI $0.05 - 0.57$). This restriction, in part, is a result of inaccessibility of the areas as healthcare workers will not be able to provide the required vaccines, thermometers and key tools for limiting EVD transmission, (Kasereka et al. 2019, Maxmen 2018). For the model developed in (Wells et al. 2019) to assess the impact of conflict on the epidemic in eastern DRC, it was observed that the effective reproduction number increased significantly above unity with attacks on healthcare workers.

In the animal kingdom, fruit bats are believed to be the normal carrier, able to spread the

virus without being affected by it (WHO 2014). In conflict ravaged areas, the communities resort to bush meat and forest based livelihoods. Furthermore, the consumption of bats, hunted meat and fruits from the forest is the norm. There is little to no subsistence farming as crops may be destroyed deliberately. Taking into account this new way for people to feed themselves, the work (Berge et al. 2017c) enriched the existing literature by incorporating indirect transmission through the contaminated environment.

There has been some progress in the use of vaccines (*e.g.* rVsV-ZEBOV-GP Ebola vaccine and Ad26.ZEBOV/MVA-BN-Filo vaccine) to combat the spread of EVD in DRC (WHO 2020*c*). In (Berge et al. 2018a), the authors broadened the work of (Berge et al. 2017c) and presented a deterministic model that incorporates the vaccinated compartment and the awareness of the population and behavioural changes. Their findings suggest that EVD can be controlled and eradicated subject to compliance with the protection measures including the vaccines. However, these efforts have often been compromised, in part, due to the ongoing war and general social resistance, which tends to support the notion of EVD potentially being used as a bio terrorism agent (Kasereka et al. 2019, Maxmen 2018, Richardson et al. 2010).

In the present work, the ability of the healthcare facility/system to accommodate infected individuals, and the escape of the latter from the facility/system are the two factors we use to assess how the presence of war and political instability in EVD endemic regions have exacerbated the spread of the disease. We construct a SIR-type deterministic model, with contaminated environment class, in which the two parameters are suitably incorporated. Escaped individuals are guided by fear and they are cautious to hide at safe places. To account for this, our model consists of two patches, one of which is less affected by the burden of EVD, war, violence, *etc.*

One of the key points of the work is the expression of both the force of infection and the basic reproduction number in which the said parameters of escaping and destroying of healthcare facility are carefully captured. On this basis, we carry out a rigorous analysis of the model, which shows how the two key parameters should vary for the basic reproduction number to be less or larger than the unity so that the disease dies out or not. From the computational point of view, we use the revisited methodology in (Anguelov et al. 2020, Mickens 2020) to construct a nonstandard finite difference (NSFD) scheme that is dynamically consistent with the continuous model. In particular, after establishing a discrete analogue of a result in (Castillo-Chavez et al. 2002) regarding the global asymptotic stability of the disease-free equilibrium, we apply it to show that our NSFD scheme preserves this property. We highlight that case studies such as the current work, have implications for the type of investments needed to enable effective response to Ebola, and other zoonotic diseases in general, in conflict affected settings.

The rest of the paper is structured as follows. In the next section, we state the main assumptions and use them to formulate the mathematical model. We estimate the parameters and fit the model to the data of the DRC 2018-2020 EVD in Section 3. Section 4 is devoted to three important aspects. Starting with the biological well-posedness of the model, we compute the basic reproduction number and establish the associated stability results, including the case

of the endemic equilibrium, which is more involved for a patch model like the one investigated here. The NSFD scheme is presented in Section 5 together with numerical simulations which support the theory. Concluding remarks as well as possible extensions of this work are discussed in Section 6.

2 Model formulation

In the absence of conflict and war, the transmission dynamics of the Ebola Virus Disease (EVD) is generally modelled in Kermack-McKendrick's framework of Susceptible-Infectious-Recovered (SIR), where the exposed class is omitted for simplicity (Berge et al. 2018a, 2017c), though considered in other studies (Agusto et al. 2015, Tsanou et al. 2017b). Thus, we assume homogeneous mixing, and recovery induced permanent natural immunity against future infections. In the current study that deals with the EVD in a war region with limited, but targeted, healthcare facility, we have to factor patients fleeing from the facility for their safety. To this end, we consider a two-patch SIR model. In Patch 1, we use an extension of the SIR model relabeled as $S_1I_1R_1$, and modified by the incorporation of the H and L classes to account for hospitalized/isolated and escaped (from hospitals) individuals, respectively. Hence, the total population a time t, $N_1(t)$, is divided into five mutually-exclusive compartments so that

$$N_1 = S_1 + I_1 + R_1 + H + L. \tag{1}$$

It should be noted that disease epidemiological models with treatment or hospital compartments are abundantly used in the literature. In this study, the H class consists of patients in all the Ebola Treatment Centres and the Ebola Transit Centres in the affected region/Patch 1. However, the incorporation of the L class, a special feature of this study, is to the authors best knowledge new. Given the severity of the EVD, the movements of patients escaping from hospitals must be carefully managed. Typically, these are wanted individuals: once patients escape, an aggressive contact tracing and call to the community are made to find them (we will come back to this in a moment).

Patch 2 is precisely the go-to area for escaped patients because it is assumed that there is neither EVD healthcare facility there, nor other resources that can attract armed groups. Hence, Patch 2 includes the forest (environment). We consider there, the classical $S_2I_2R_2$ model with

$$N_2 = S_2 + I_2 + R_2, \tag{2}$$

for the total population $N_2(t)$ at time t. The total population $N(t)$ at time $t \geq 0$ in the two patches satisfies

$$N = N_1 + N_2. \tag{3}$$

Due to the nature of the EVD, deceased individuals significantly contribute to the spread of the virus, see for example (Berge et al. 2018a), and the literature therein. Thus, we add to each

patch the deceased class, D_i, for $i = 1, 2$. Finally, we consider the contaminated environment classes, P_1 and P_2, corresponding to the two patches. Each P_i $(i = 1, 2)$ is the concentration of the virus in the environment due to shedding by the deceased and infectious individuals in patch i. Though it is possible for the two patches to have a common source of environmental contamination (Shuai & Van den Driessche 2015), we use two sources, which is biologically more reasonable.

Susceptible individuals contract infection either directly by contact with infectious, escaped and deceased individuals, or indirectly through the contaminated environment. Therefore, the force of infections for the patches are given by

$$\lambda_1 = \beta_1 \left(\frac{I_1 + \epsilon L}{N_1} + \epsilon_1 D_1 \right) + \beta_3 P_1, \tag{4}$$

and

$$\lambda_2 = \beta_2 \left(\frac{I_2 + \epsilon \nu L}{N_2 + \nu L} + \epsilon_2 D_2 \right) + \beta_3 P_2, \tag{5}$$

where β_1, β_2 and β_3 (for the environment) are the associated contact rates, while ϵ_1, ϵ_2 and ϵ (for the escape class) are the modification parameters. Note that we use the mass action principle for the deceased individuals and environment variables as in (Berge et al. 2017c, 2018a) and some other works in the literature ; but the standard incidence is implemented for the I_i & L classes on the understanding that, for the cross infection from Patch 1 to Patch 2, the effective and updated total population in Patch 2 is used as in for instance (Bichara & Iggidr 2018, Iggidr et al. 2012).

In each patch, the susceptible class S_i increases by a constant recruitment Λ_i, and decreases at the rates λ_i and μ, where μ is the natural death rate for each human class. Thus the evolution in time of susceptible individuals is modeled by the differential equation

$$\frac{dS_i}{dt} = \Lambda_i - (\lambda_i + \mu) S_i.$$

Individuals who have contracted EVD are hospitalised and classified under the epidemiological class H at the rate $\alpha_1(1 - \tau)$, where τ is the (dimensionless) parameter of destruction of healthcare facility. However, due to the perceived risk associated with staying in hospitals, individuals escape these facilities at the rate ξ and move into the epidemiological class L. Some Individuals in L class go back into hospital at the rate φ, some moved into I_1 class in patch one at the rate f and some escape into class I_2 in patch two with rate ν. With the above and taking into account the natural death of all humans at the rate μ, the differential equation for the escape class is readily found to be

$$\frac{dL}{dt} = \xi H - (f + \varphi + \nu + \mu + \delta) L,$$

where δ, the disease-induced death rate, is assumed to be the same for hospitalized individuals not only for simplicity but especially because there is as such no confirmed and effective medication against EVD. Though there seems to be no direct benefit to hospitalized individuals

in terms of disease-induced death, there is non negligible gain at the community level because hospitals, as isolation centres, prevent patients from spreading the disease. Hence, the focus in what follows is on patients who escape the hospitals.

In each patch, there are two contributions to the increase of the I_i infectious class. These are the new infectious from the S_i class at the rate λ_i and the escape individuals in L class that move back to the I_1 class and the I_2 class at the rates f and ν, respectively. However, there are four contributions to the decrease of the I_i class. The first contribution is that of individuals in the I_1 and I_2 classes hospitalized at the rates $\alpha_1(1-\tau)$ and α_2, respectively. Then follow the recovery individuals at the rate γ_i (γ_3 for hospitalized individuals), and the natural and disease-induced deaths at the rates μ and δ, respectively. These comments lead to the following differential equations for the infectious classes:

$$\begin{cases} \dfrac{dI_1}{dt} = \lambda_1 S_1 + fL - (\alpha_1(1-\tau) + \gamma_1 + \mu + \delta)\, I_1, \\ \dfrac{dI_2}{dt} = \lambda_2 S_2 + \nu L - (\alpha_2 + \gamma_2 + \mu + \delta)\, I_2. \end{cases}$$

From all the above comments, the following differential equations for the hospitalized and recovered classes are also obtained in a straight forward manner:

$$\begin{cases} \dfrac{dH}{dt} = \alpha_1(1-\tau)I_1 + \alpha_2 I_2 + \varphi L - (\xi + \gamma_3 + \mu + \delta)H \\ \dfrac{dR_1}{dt} = \gamma_1 I_1 + \gamma_3 H - \mu R_1 \\ \dfrac{dR_2}{dt} = \gamma_2 I_2 - \mu R_2. \end{cases}$$

As noted earlier, patients who escape from hospitals are wanted. Once found, their readmission to the hospitals is prioritized. It is also a priority to manage individuals infected by escaped patients. They are placed in one of the hospitals, which is always possible because all the 36 Ebola Treatment and Transit Centres across the affected region cannot be destroyed at the same time. In other words, the parameter τ does not reach the value 1 in practice. Hence, unlike the coefficient α_1, the hospitalization rates, φ and α_2 are not multiplied by $1-\tau$ in the above differential equation model of the H variable.

At this stage, it is important to stress again that the recruitment in each sub-population is through the susceptible class, while migration between the two sub-populations is only by infected individuals escaping from the healthcare facilities. Furthermore, it is clear that the two patches are coupled *via* the residence time $1/\nu$.

Recording all death individuals from the I_i, H, and L evolution equations, we obtain the following differential equations for the deceased classes:

$$\begin{cases} \dfrac{dD_1}{dt} = (\mu + \delta)(I_1 + H + L) - bD_1 \\ \dfrac{dD_2}{dt} = (\mu + \delta)I_2 - bD_2, \end{cases}$$

where b^{-1} is the mean caring duration of EVD deceased individuals.

Apart from H, all classes I_1, I_2, D_1, D_2 and L with infection shed the virus in the environment, P_1 (Patch 1) and P_2 (Patch 2), at the rates $\{\eta_{2k+1}\}_{0\leq k\leq 2}$ and $\{\eta_{2k}\}_{1\leq k\leq 2}$, respectively. The decay rate of the virus in both patches are the same, θ. Thus, the differential equations for P_1 and P_2 classes are

$$\begin{cases} \dfrac{dP_1}{dt} = \eta_1 I_1 + \eta_3 D_1 + \eta_5 L - \theta P_1, \\ \dfrac{dP_2}{dt} = \eta_2 I_2 + \eta_4 D_2 - \theta P_2. \end{cases}$$

The flow diagram for the transmission dynamics of EVD is depicted in Figure 3 and descriptions of state variables and parameters used in the model are given on Table 2. In

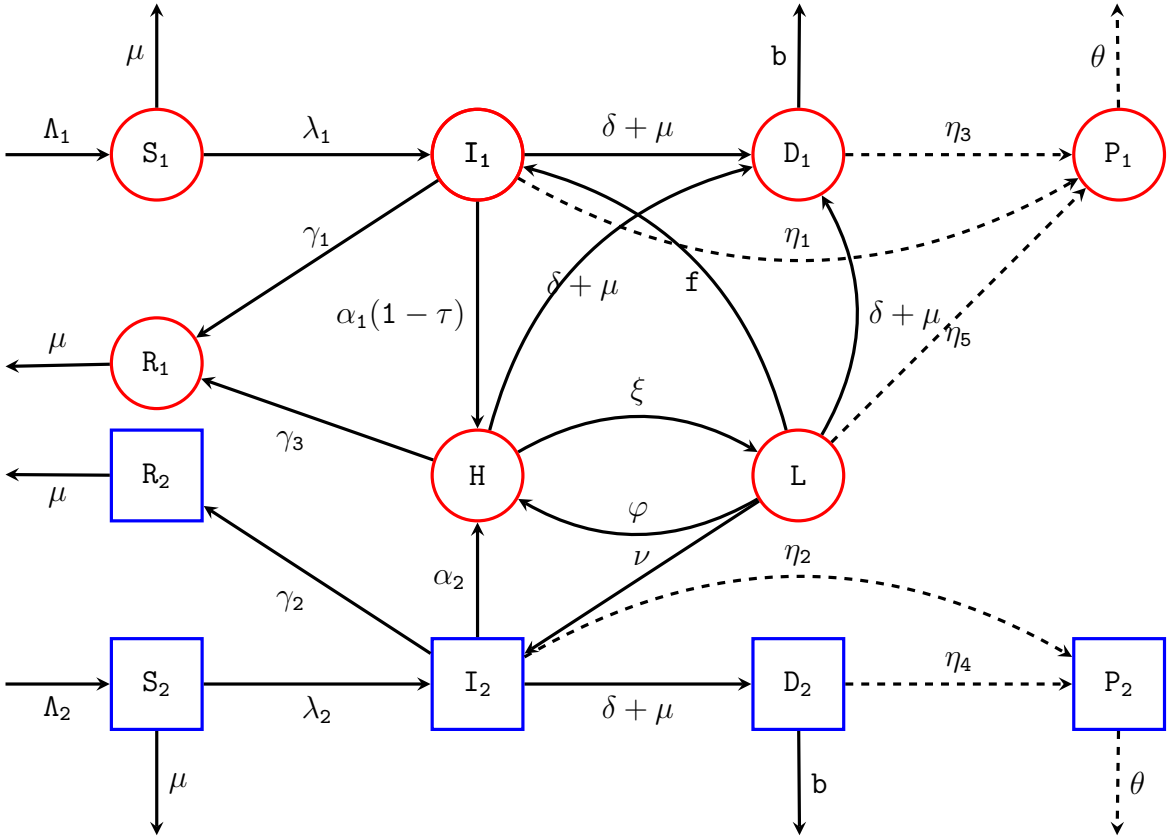

Figure 3: Schematic diagram of the two-patch model of EVD transmission.

summary, we obtain the following system of nonlinear ordinary differential equations for the transmission dynamics of the Ebola Virus Disease:

$$
\begin{cases}
\dfrac{dS_1}{dt} = \Lambda_1 - (\lambda_1 + \mu)S_1 \\
\dfrac{dI_1}{dt} = \lambda_1 S_1 + fL - k_1 I_1, \\
\dfrac{dH}{dt} = \alpha_1(1-\tau)I_1 + \alpha_2 I_2 + \varphi L - k_2 H, \\
\dfrac{dL}{dt} = \xi H - k_3 L, \\
\dfrac{dR_1}{dt} = \gamma_1 I_1 + \gamma_3 H - \mu R_1, \\
\dfrac{dD_1}{dt} = k_4(I_1 + H + L) - bD_1, \\
\dfrac{dP_1}{dt} = \eta_1 I_1 + \eta_3 D_1 + \eta_5 L - \theta P_1,
\end{cases} \tag{6}
$$

$$
\begin{cases}
\dfrac{dS_2}{dt} = \Lambda_2 - (\lambda_2 + \mu)S_2, \\
\dfrac{dI_2}{dt} = \lambda_2 S_2 + \nu L - k_5 I_2, \\
\dfrac{dR_2}{dt} = \gamma_2 I_2 - \mu R_2, \\
\dfrac{dD_2}{dt} = k_4 I_2 - bD_2, \\
\dfrac{dP_2}{dt} = \eta_2 I_2 + \eta_4 D_2 - \theta P_2,
\end{cases} \tag{7}
$$

where the constants k_i are defined as follows:

$$
k_1 = \alpha_1(1-\tau) + \gamma_1 + k_4,\ k_2 = \xi + \gamma_3 + k_4,\ k_3 = f + \varphi + \nu + k_4, \text{ and } k_5 = \alpha_2 + \gamma_2 + k_4, \tag{8}
$$

with $k_4 = \mu + \delta$. The system (6)-(7) is appended with the following non-negative initial conditions for the dependent variables and the total population and sub-population: for $i = 1,\ 2,$

$$
(S_i(0), I_i(0), H(0), L(0), R_i(0), D_i(0), P_i(0)) = (S_0^i, I_0^i, H_0, L_0, R_0^i, D_0^i, P_0^i);\ N(0) = N_0;
$$
$$
N_i(0) = N_0^i.
$$

Remark 2.1. *The importance of the parameter τ in the model (6)-(7) needs to be highlighted, though some focused comments were made earlier. In the normal case, $\tau = 0$, where there is no war, violence, attacks, etc., the hospitals are fully operational to admit EVD patients. The extreme case or the limit, $\tau = 1$, is not reached in practice because it corresponds to the unlikely scenario where all the Ebola treatment and transit centres in the affected region are destroyed. This unlikely scenario ($\tau = 1$) also implies that the hospitalized class, H, and the escape class, L, become zero, reducing the model to a simplified Patch 1 model. The situation when $0 < \tau < 1$, is the most realistic one and it corresponds to the hospitals being partially operational (see also Remark 4.2). This will be illustrated in the numerical simulations section.*

Variable	Description
$S_1(S_2)$	Class of susceptible individuals in the first (second) patch
$I_1(I_2)$	Class of infected individuals in the first (second) patch
H	Class of infected individuals who are hospitalised in the first patch
L	Class of infected individuals escaped from hospital
$R_1(R_2)$	Class of recovered individuals in the first (second) patch
$D_1(D_2)$	Class of deceased individuals in the firs (second) patch
$P_1(P_2)$	Class of Ebola virus contaminated environment in Patch 1 (Patch 2)
Parameter	**Description**
$\Lambda_1(\Lambda_2)$	Recruitment rate of susceptible individuals in the first (second) patch
$\gamma_1(\gamma_2)$	Rate of recovery for $I_1(I_2)$ class
γ_3	Rate of recovery for H class
μ	Natural death rate
δ	Ebola induced death rate
$\alpha_1(\alpha_2)$	Rate of individuals to be hospitalised in patch one from patch one (two)
$1/b$	Mean caring duration of Ebola deceased human individuals
$\beta_1(\beta_2)$	Contact rate for first (second) patch
β_3	Contact rate for ebola virus contaminated environment
$\epsilon_1,\ \epsilon_2$	Modification parameters
$\eta_1,\ \eta_3,\ \eta_5$	Shedding rates of $I_1,\ D_1$ and L classes to the P_1 class, respectively
$\eta_2,\ \eta_4$	Shedding rates of I_2 and D_2 classes to the P_2 class, respectively
θ	Decay rate of Ebola virus in the environment
ξ	Rate of escaping from hospital/healthcare facility
f	Rate of escaped individuals from L moving into I_1 class
φ	Rate of escaped individuals from L moving back into H class
ν	Fraction of individuals in class L moving into the second patch
ϵ	Modification parameter for νL individuals in patch two
τ	Parameter of destruction of healthcare facility in a war zone

Table 2: Description of parameters of the model (6)-(7).

3 Estimation of parameters and model fitting

From the DRC provinces map and the EVD distribution map in Figure 1, we assume that Patch 1 consists of Ituri, North Kivu and South Kivu provinces, while Patch 2 is formed by their neighbouring provinces of Haut Uele, Tshopo and Maniema where there were no EVD.

In 2019, the total population of Patch 1 was estimated at $23,151,520$ including $6,075,486$ (Ituri Province), $9,211,041$ (North Kivu Province) and $7,864,993$ (South Kivu), as *per* the report (DRC Ministry 2021). The same source reports that the total population of Patch 2 was $8,603,545$ ($2,168,709$ for Haut Uele Province, $2,830,392$ for Maniema Province and $3,604,444$ for Tshopo Province). Since the population growth rate by birth in DRC is estimated at 40.639 *per* 1000 people (World Bank 2019*a*), we estimate the recruitment of susceptible individuals *per* day in Patch 1 at $\Lambda_1 = (40.639 \times 23,151,520)/(1000 \times 365) = 2578$. Likewise, for Patch 2, we have the estimate $\Lambda_2 = 978$. The natural mortality in DRC being estimated at 9.292 deaths *per* 1000 inhabitants in 2019, the annual natural death rate is 0.92892% and thus we have the estimate $\mu = 0.00003$ *per* day.

Under the African culture, it normally takes 1 - 7 days for the burial or cremation of deceased individuals. This gives an estimate for b in the range $[0.14, 1]$ *per* day. Our baseline value is assumed to be 0.8

The parameter $1/\alpha_1(1/\alpha_2)$ denotes the average time from symptom to onset to hospital admission. Here, we assume this to be $[4.71, 7.32]$ days as given in (Wells et al. 2019). That is $\alpha_1(\alpha_2)$ ranges between $0.137 - 0.212$ *per* day. The time to death from symptom onset of Ebola disease ranges between 7.25 to 13.5 days (Siewe et al. 2020), *i.e.*, δ ranges between $0.074 - 0.138$ *per* day. The case fatality of Ebola varies between 20% to 90%, see for example (Siewe et al. 2020). Using estimates from (Siewe et al. 2020), we take the time to recovery from Ebola to be 3.10 to 7.84 days, *i.e.*, $\gamma_1(\gamma_2)$ ranges between $0.13 - 0.32$ *per* day.

We now come to the difficult task of estimating the parameters that are related to the impact of war and conflict. From the appendix and supplementary information provided in (Wells et al. 2019), we have constructed the expanded Table 3, which gathers the number of disruptive events for the period of twelve months, *i.e.*, from 1 September 2018 to 31 August 2019. We classify the disruptive events into two categories. The first category consists of Events that Incapacitate the Healthcare System (EIHS), namely "ville morte" [dead/ghost city] day, attacks of healthcare workers (HCW), attacks of ETC, and healthcare workers protests. The second category, OTHERS, consists of all other events including mainly the escape of patients from hospitals. Note that July and August 2019, the disruptive events of which are described in (Reliefweb 2019), were not included in (Wells et al. 2019). Since we could not find any reports giving the breakdown *per* month of disruptive events for the rest of the year 2019, we limited the table to August 2019, though a summary of these sad events as well as the numbers of cases and deaths for the entire period are provided in references (Reliefweb 2021) and (WHO 2019*c*), respectively.

Description	Sep 18	Oct 18	Nov 18	Dec 18	Jan 19	Feb 19	Mar 19	Apr 19	May 19	Jun 19	Jul 19	Aug 19
Event												
Ville morte	1	1	0	0	0	0	0	0	0	3	0	0
Attack HCW	0	2	0	0	2	3	1	1	2	3	3	2
HCW protest	0	0	1	0	0	1	1	1	0	0	0	0
Attack ETC	0	0	0	5	0	5	4	2	6	2	1	2
Others	0	0	0	0	0	1	0	3	0	0	0	1
Sub-total	**1**	**3**	**1**	**5**	**2**	**10**	**6**	**7**	**8**	**8**	**4**	**5**
Total												**60**
Impact												
Cases	150	216	300	585	699	872	1016	1353	1920	2239	2671	2976
Deaths	100	139	186	356	433	548	634	880	1281	1510	1790	1990

Table 3: Disruptive events in the most affected health zones and impact on the number of deaths from the pool of total cases

The numbers of cases and deaths retained on the table are taken from WHO external situations reports, (WHO 2019*c*); they correspond to those of the date or the closest date in the month when the disruptive event occurred. For example, the external situation report no. 21 (2018) reports 585 cases and 356 deaths on 27 December 2018, which, for the last four months of the year 2018, turns out to be the date when both the peak of the disease was reached and ETCs were seriously attacked (BBC News 2018, Wells et al. 2019). We emphasize the link between the incidence of conflict and observed cases by calculating the Pearson's correlation coefficient, ρ, between "cases" and Total EIHS. Here we have $\rho = 0.43$, which suggests a very strong linear correlation between the two data sets. In so doing, we can visualize the impact of the disruptive events to compromise the ability of the healthcare system to control and manage the EVD. The table reveals indeed that the more the attacks of ETCs, the highest are the numbers of new cases and deaths; the situation becomes worse in the presence of additional disruptive events (see Dec18 and Feb19 columns, respectively).

For further assessment of the impact of war/conflict on the control of the EVD, it seems reasonable to include on Table 3 a row tabulating the number of patients admitted to ETCs *per* month. We could unfortunately not get this information. Nevertheless, the narratives of a couple of days when ETCs were attacked are illustrative of the trauma created on admitted patients, and the number of those who left the healthcare facility. For instance, the attack on 27 December 2018 of Médecins Sans Frontières' [Doctors Without Borders'] transit center in Beni resulted in 9 of the 28 patients to spontaneously leave the center (see article, video and flyer in (Médecins Sans Frontières 2021*b*)).

Despite the comments and the attempt made in the previous two paragraphs, the question of formulating precisely the correlation between disruptive events and the number of cases and

deaths is not easy! Based on the data on Table 3 and using the acronyms EIHS and OTHERS defined above, we propose here a relatively simple method to estimate the key parameters τ and ξ that capture the impact of the war/conflict in our model. We introduce the following formula:

$$\tau|_{\text{ month}} := q\frac{(\text{Total EIHS})|_{\text{month}}}{(\text{Total Events})|_{\text{month}}} \text{ and } \xi|_{\text{ month}} := \frac{(\text{Total OTHERS})|_{\text{month}}}{(\text{Total Events})|_{\text{month}}}$$

where q is the probability for a disruptive event to incapacitate the healthcare system. We then take the baseline values of τ and ξ to be the averages of $\tau|_{\text{month}}$ and $\xi|_{\text{month}}$, *i.e.*

$$\tau = \frac{\sum \tau|_{\text{month}}}{12} = 0.313 \text{ and } \xi = \frac{\sum \xi|_{\text{month}}}{12} = 0.061 \tag{9}$$

by using the data on the Table 3 and assuming that $q = 1/3$, based on our rough counting from (Wells et al. 2019) of closures and suspensions of activities of healthcare facility. Furthermore, we assume that the parameters τ and ξ vary in the intervals $[0, \max\{\tau|_{\text{month}}\}]$ and $[0, \max\{\xi|_{\text{month}}\}]$, respectively, *i.e.*

$$\tau \in [0,\ 0.33] \text{ and } \xi \in [0,\ 0.43]. \tag{10}$$

From the explanation given above on the counting of data on Table 3, it should be noted that the notation $\tau|_{\text{ month}}$ and $\xi|_{\text{ month}}$ actually refers to one day in the month.

For the parameters φ, ν and f that determine the fate of patients that escape from the healthcare facility, and in view of Eqs (9)-(10), we take

$$\varphi = \nu = f = \frac{\xi}{3} = 0.02, \tag{11}$$

as corresponding baseline values, while the range of these parameters is as follows:

$$\varphi,\ \nu,\ f \in [0, 0.143]. \tag{12}$$

Finally, we estimate the range of the shedding parameters η_i $(i = 1, \cdots, 5)$, the contact rates β_i $(i = 1, \cdots, 3)$, and the modification parameters ϵ_i $(i = 1,\ 2)$ and ϵ. This will essentially be done by fitting our model to the reported deaths as explained below. It is well known that the Ebola virus can survive for several days in the environment. This is the case for the Zaire-type Ebola virus that survived 14 days at $4°C$ on glass, plastic and surfaces (Bibby et al. 2015). Furthermore, $0.1 - 1\%$ of Ebola virus remained active for up to 50 days at $4°C$, as reported in (Piercy et al. 2010). In view of this fact, and taking into account some necessary fitting, we assume that the five parameters η_i vary in the much smaller interval $[1 \times 10^{-9}, 1 \times 10^{-5}]$. However, their estimated baseline values as well as those of the three parameters β_i and $\epsilon, \epsilon_1, \epsilon_2$ are fitted using the reported number of deaths on Table 3. This is motivated by the following facts:

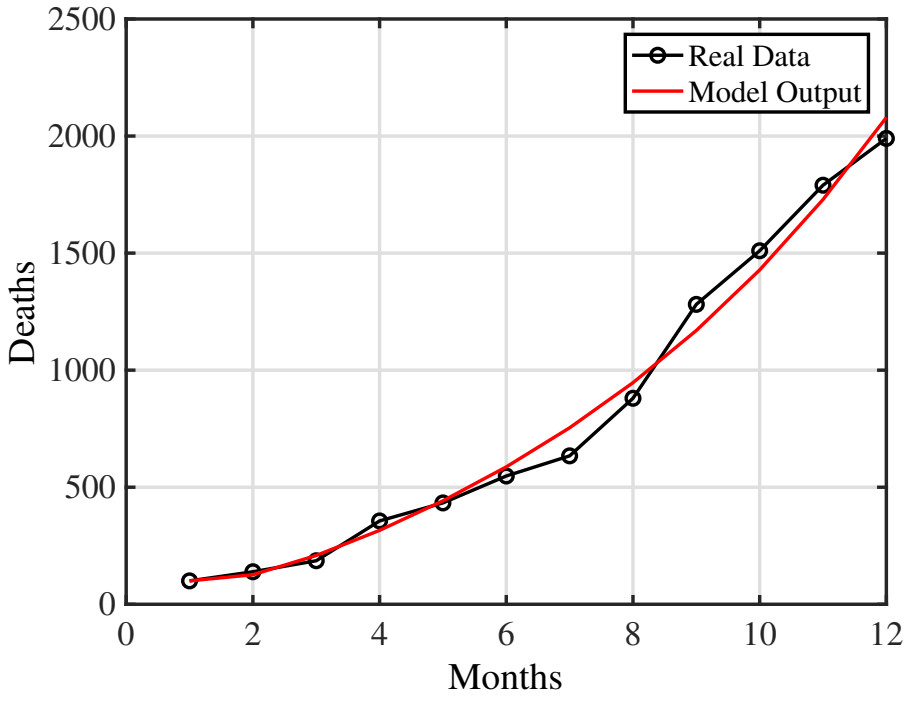

Figure 4: Model fitting to the cumulative number of reported deaths from Table 3.

1. The overall disruptive events took place in the three provinces that form Patch 1. Therefore, it is reasonable to fit the involved parameters $\beta_1, \beta_3, \epsilon_1, \epsilon, \eta_1, \eta_3, \eta_5, \epsilon_1$ and deduce the corresponding parameters for Patch 2.

2. Biologically/epidemically, there is no reason for infected individuals and Ebola-deceased individuals from the two patches to shed the virus differently in the environment. Consequently, we assume that $\eta_2 = \eta_1$ and $\eta_4 = \eta_3$ for Patch 2.

3. Similarly to the previous item, there is no biological/epidemiological evidence for the modification parameter ϵ_1 in Patch 1 to be different from its analogue ϵ_2 in Patch 1. Therefore, we assume that $\epsilon_1 = \epsilon_2$ during the curve fitting process.

4. Patch 1 being the most affected region by disruptive events, it is reasonable to assume that individual daily contact behavior in Patch 1 is drastically restricted in contrast to the situation in Patch 2 where the normal African tradition prevails. Therefore, once Patch 1 contact rate β_1 is fitted, we assume Patch 2 contact rate is larger *i.e.* $\beta_2 = m\beta_1$, with $m > 1$ to be fitted.

5. For the environment, it is observed that the parameter β_3 is sensitive, see (Berge et al. 2018a). Therefore, by differentiating the environmental infection from Patch 1 and Patch 2, we assume the range of β_3 is $[1 \times 10^{-5}, 1 \times 10^{-4}]$.

6. Finally, we assume that the initial susceptible sub-population in the two patches correspond to their respective total populations while initially in Patch 1, there are 900

infected individuals, 5 hospitalised and 5 escapees. In Patch 2, we assume that there are 5 infected individuals (corresponding to those who escaped the hospitals in Patch 1).

For convenience, all calculated, estimated and fitted values of the parameters are gathered on Table 4, and will be used later for all numerical simulations.

The parameter fitting process was based on a nonlinear least squares algorithm implemented by using *"fminsearchbnd"* function in MatLab. The advantage of using *"fminsearchbnd"* instead of *"fminsearch"* is that the latter enables us to keep the fitted parameters in their estimated ranges. It consisted in minimizing the sum of the squares of the difference between the predictions of the cumulative deaths in the full model and the reported cumulative deaths available on Table 3 for a 12-month period ranging from September 2018 to August 2019. Figure 4 shows a good fit of the full model to the cumulative number of reported deaths given in Table 3.

Parameter	**Range**	**Baseline value**	**Source**
$\Lambda_1(\Lambda_2)$		2578 (978)	Calculated based on (DRC Ministry 2021, World Bank 2019*a*)
$\gamma_1(\gamma_2)$	[0.13,0.32]	0.3	Calculated based on (Siewe et al. 2020)
γ_2	[0.13,0.32]	0.2002	Fitted
γ_3	[0.06,0.12]	0.1	Assumed
μ		0.00003	Calculated based on (DRC Ministry 2021, World Bank 2019*a*)
δ	[0.074,0.138]	0.1	(Siewe et al. 2020)
α_1	[0.137,0.485]	0.2(0.2)	Calculated based on (Wells et al. 2019)
α_2	[0.137,0.485]	0.15	Fitted
b	$[0.14, 1]$	0.8	Calculated as *per* African burial culture
θ	$[0.0155, 0.030]$	0.03	(Bibby et al. 2015)
ξ	[0, 0.43]	0.061	Estimated from Eqs (9)-(10) and Table 3
f, φ, ν	[0, 0.143]	0.02	Estimated from Eqs (11)-(12) and Table 3
τ	[0, 0.33]	0.313	Estimated from Eqs (9)-(10) and Table 3
β_1	$[1\times10^{-3}, 1.7\times10^{-2}]$	1.680×10^{-2}	Fitted
β_2	$[1\times10^{-3}, 1.5\times10^{-2}]$	1.489×10^{-2}	Fitted ($\beta_2 = m\beta_1$, with $m = 1.363$)
β_3	$[1\times10^{-4}, 3.2\times10^{-3}]$	3.173×10^{-3}	Fitted
ϵ_1		4.824×10^{-6}	Fitted
ϵ_2		4.824×10^{-6}	Fitted
η_1	$[1\times10^{-9}, 1\times10^{-5}]$	2.721×10^{-9}	Fitted
η_2	$[1\times10^{-9}, 1\times10^{-5}]$	2.721×10^{-9}	Fitted
η_3	$[1\times10^{-11}, 1\times10^{-5}]$	7.938×10^{-11}	Fitted
η_4	$[1\times10^{-11}, 1\times10^{-5}]$	7.938×10^{-11}	Fitted
η_5	$[1\times10^{-11}, 1\times10^{-5}]$	9.856×10^{-11}	Fitted
ϵ		0.002892	Fitted

Table 4: Calculated, estimated, fitted and baseline parameter values for the model. Their description is provided in Table 2.

4 Quantitative and qualitative analysis

We start this section with the well-posedness of the proposed model.

Theorem 4.1. *The EVD model (6)-(7) is a dynamical system on the biologically feasible region* Ω *defined by*

$$\Omega = \left\{(S_1, I_1, H, L, R_1, D_1, P_1, S_2, I_2, R_2, D_2, P_2) \in \mathbb{R}_+^{12} : 0 \leq N \leq \frac{\Lambda}{\mu},\ 0 \leq D \leq \frac{K}{b} \text{ and } 0 \leq P \leq \frac{\Pi}{\theta}\right\}$$

where $\Lambda = \Lambda_1 + \Lambda_2$, $D = D_1 + D_2$, $P = P_1 + P_2$, $K = (\delta + \mu)\Lambda/\mu$ *and* $\Pi = (\eta_1 + \eta_2 + \eta_5)\frac{\Lambda}{\mu} + (\eta_3 + \eta_4)K/b$. *Furthermore, the region* Ω *is attracting with respect to the system (6)-(7) with initial conditions in* $\mathbb{R}_+^{12}$.

Proof: We want to show that for non-negative initial data, the system (6)-(7) possesses at all time $t \geq 0$, a unique non-negative solution which lies in the region Ω. The proof will follow two steps.

The positive cone $\mathbb{R}_+^{12}$ is invariant for the system (6)-(7) by using the tangent condition or barrier theorem for each hyper-plane of the boundary $\partial\mathbb{R}_+^{12}$ (Busenberg & Cooke 2012, Walter 2012).

In a second step, we show that any solution of the model system (6)-(7) satisfies some *a priori* estimates. By adding the equations in (6)-(7) related to the classes of individuals involved in the defining equations (1)-(3), we obtain the conservation law

$$\frac{dN}{dt} = \Lambda - \mu N - \delta(H + L + I_1 + I_2), \tag{13}$$

from which it follows that

$$\frac{dN}{dt} \leq \Lambda - \mu N. \tag{14}$$

Applying Gronwall inequality to (14) leads to

$$N(t) \leq \frac{\Lambda}{\mu} + \left(N_0 - \frac{\Lambda}{\mu}\right)\exp(-\mu t). \tag{15}$$

From (15) , we have

$$0 \leq N(t) \leq \frac{\Lambda}{\mu} \quad \text{for} \quad 0 \leq N_0 \leq \frac{\Lambda}{\mu}. \tag{16}$$

Likewise, with K defined above, applying Gronwall inequality to the sum of two deceased classes in (6)-(7) yields

$$D(t) \leq \frac{K}{b} + (D_0 - \frac{K}{b})\exp(-bt). \tag{17}$$

from which we infer that, for any time $t \geq 0$,

$$0 \leq D(t) \leq \frac{K}{b} \quad \text{whenever} \quad 0 \leq D_0 \leq \frac{K}{b}. \tag{18}$$

Finally, the sum of the last two equations of (6)-(7) gives

$$\frac{dP}{dt} = \eta_1 I_1 + \eta_3 D_1 + \eta_5 L + \eta_2 I_2 + \eta_4 D_2 - \theta P \leq \Pi - \theta P. \tag{19}$$

Once again, Gronwall inequality applied to (19) with $P(0) = P_0$, leads to

$$0 \leq P(t) \leq \frac{\Pi}{\theta} + \left(P_0 - \frac{\Pi}{\theta}\right) \exp(-\theta t), \tag{20}$$

so that

$$0 \leq P(t) \leq \frac{\Pi}{\theta}$$

for all $t > 0$, whenever $0 \leq P_0 \leq \dfrac{\Pi}{\theta}$.

When a solution of the system starts outside Ω, with $N_0 > \Lambda/\mu$ or $D_0 > K/b$ or $P_0 > \Pi/\theta$, it follows from (15), (17) and (20) that $\limsup_{t\to\infty} N(t) \leq \Lambda/\mu$, $\limsup_{t\to\infty} D(t) \leq K/b$ and $\limsup_{t\to\infty} P(t) \leq \Pi/\theta$. Hence, the region Ω is attracting.

Combining the above two steps and using Theorem 2.1.5 in (Stuart & Humphries 1998), we conclude that (6)-(7) defines a dynamical system on Ω. This completes the proof. □

Next, we investigate the stability of the disease-free equilibrium (DFE) of the model. To determine the DFE, we set the right-hand side of system (6)-(7) equal to zero:

$$\begin{aligned}
\Lambda_1 - (\lambda_1 + \mu)S_1 &= 0,\\
\lambda_1 S_1 + fL - k_1 I_1 &= 0,\\
\alpha_1(1-\tau)I_1 + \alpha_2 I_2 + \varphi L - k_2 H &= 0,\\
\xi H - k_3 L &= 0,\\
\gamma_1 I_1 + \gamma_3 H - \mu R_1 &= 0,\\
k_4(I_1 + H + L) - bD_1 &= 0,\\
\eta_1 I_1 + \eta_3 D_1 + \eta_5 L - \theta P_1 &= 0,\\
\Lambda_2 - (\lambda_2 + \mu)S_2 &= 0,\\
\lambda_2 S_2 + \nu L - k_5 I_2 &= 0,\\
\gamma_2 I_2 - \mu R_2 &= 0,\\
k_4 I_2 - bD_2 &= 0,\\
\eta_2 I_2 + \eta_4 D_2 - \theta P_2 &= 0,
\end{aligned} \tag{21}$$

It is readily seen that system (21) has a unique DFE, which is given by

$$E_0 = (S_1, I_1, H, L, R_1, D_1, P_1, S_2, I_2, R_2, D_2, P_2) = \left(\frac{\Lambda_1}{\mu}, 0, 0, 0, 0, 0, 0, \frac{\Lambda_2}{\mu}, 0, 0, 0, 0\right). \tag{22}$$

The basic reproduction number, $\mathcal{R}_0$, defined as the average number of secondary cases produced by one infectious individual during his/her entire infectious period in a completely

susceptible population (Van den Driessche & Watmough 2008), is an important threshold quantity for the stability analysis of the model. This number is determined by using the next generation matrix method developed in (Diekmann & Heesterbeek 2000, Van den Driessche & Watmough 2008), with extensions to some models such as those involving free living pathogens in the environment (Bani-Yaghoub et al. 2012, Shuai et al. 2013).

Using the abbreviation $X = (I_1, H, L, D_1, P_1, I_2, D_2, P_2)$ for the dependent variables with infections, we have the vector functions

$$\mathcal{F}(X) = \begin{pmatrix} \lambda_1 S_1 \\ 0 \\ 0 \\ 0 \\ 0 \\ \lambda_2 S_2 \\ 0 \\ 0 \end{pmatrix} \quad \text{and} \quad \mathcal{V}(X) = \begin{pmatrix} -fL + k_1 I_1 \\ -\alpha_1(1-\tau)I_1 - \alpha_2 I_2 - \varphi L + k_2 H \\ -\xi H + k_3 L \\ -k_4(I_1 + H + L) + bD_1 \\ -\eta_1 I_1 - \eta_3 D_1 - \eta_5 L + \theta P_1 \\ -\nu L + k_5 I_2 \\ -k_4 I_2 + bD_2 \\ -\eta_2 I_2 - \eta_4 D_2 + \theta P_2 \end{pmatrix}$$

that represent the rate of appearance of new infections and the rate of transfer of individuals among the infective classes, respectively. The constants k_i, $i = 1, \ldots, 5$ are defined in (8). The next generation matrix is given by

$$\mathcal{K} = J_{\mathcal{F}} J_{\mathcal{V}}^{-1}, \tag{23}$$

where

$$J_{\mathcal{F}} = \begin{pmatrix} \beta_1 & 0 & \beta_1\epsilon & \beta_1\frac{\epsilon_1\Lambda_1}{\mu} & \beta_3\frac{\Lambda_1}{\mu} & 0 & 0 & 0 \\ 0 & 0 & 0 & 0 & 0 & 0 & 0 & 0 \\ 0 & 0 & 0 & 0 & 0 & 0 & 0 & 0 \\ 0 & 0 & 0 & 0 & 0 & 0 & 0 & 0 \\ 0 & 0 & 0 & 0 & 0 & 0 & 0 & 0 \\ 0 & 0 & \beta_2\epsilon\nu & 0 & 0 & \beta_2 & \beta_2\frac{\epsilon_2\Lambda_2}{\mu} & \beta_3\frac{\Lambda_2}{\mu} \\ 0 & 0 & 0 & 0 & 0 & 0 & 0 & 0 \\ 0 & 0 & 0 & 0 & 0 & 0 & 0 & 0 \end{pmatrix}$$

and

$$J_{\mathcal{V}} = \begin{pmatrix} k_1 & 0 & -f & 0 & 0 & 0 & 0 & 0 \\ -\alpha_1(1-\tau) & k_2 & -\varphi & 0 & 0 & -\alpha_2 & 0 & 0 \\ 0 & -\xi & k_3 & 0 & 0 & 0 & 0 & 0 \\ -k_4 & -k_4 & -k_4 & b & 0 & 0 & 0 & 0 \\ -\eta_1 & 0 & -\eta_5 & -\eta_3 & \theta & 0 & 0 & 0 \\ 0 & 0 & -\nu & 0 & 0 & k_5 & 0 & 0 \\ 0 & 0 & 0 & 0 & 0 & -k_4 & b & 0 \\ 0 & 0 & 0 & 0 & 0 & -\eta_2 & -\eta_4 & \theta \end{pmatrix}.$$

are the Jacobian matrices of $\mathcal{F}$ and $\mathcal{V}$ at E_0, respectively. Mathematically, $\mathcal{R}_0$ is equal to $\rho(\mathcal{K})$, the spectral radius of the matrix in (23). As seen below, the computation of the matrix $\mathcal{K}$ is quite involved due to the strong non-linearity of the model. Indeed:

$$J_{\mathcal{V}}^{-1} = \begin{pmatrix} \frac{Q_1}{Q_0} & \frac{fk_5\xi}{Q_0} & \frac{fk_2k_5}{Q_0} & 0 & 0 & \frac{f\xi\,\alpha_2}{Q_0} & 0 & 0 \\ \frac{\alpha_1(1-\tau)k_5k_3}{Q_0} & \frac{k_5k_3k_1}{Q_0} & \frac{Q_2}{Q_0} & 0 & 0 & \frac{\alpha_2k_3k_1}{Q_0} & 0 & 0 \\ \frac{(1-\tau)k_5\xi\,\alpha_1}{Q_0} & \frac{k_1k_5\xi}{Q_0} & \frac{k_2k_1k_5}{Q_0} & 0 & 0 & \frac{\xi\,\alpha_2k_1}{Q_0} & 0 & 0 \\ \frac{Q_3}{bQ_0} & \frac{Q_4}{bQ_0} & \frac{Q_5}{bQ_0} & b^{-1} & 0 & \frac{Q_6}{bQ_0} & 0 & 0 \\ \frac{Q_7}{b\theta\,Q_0} & \frac{Q_8}{b\theta\,Q_0} & \frac{Q_9}{b\theta\,Q_0} & \frac{\eta_3}{b\theta} & \theta^{-1} & \frac{Q_{10}}{b\theta\,Q_0} & 0 & 0 \\ \frac{\nu\,\xi\,\alpha_1(1-\tau)}{Q_0} & \frac{\nu\,k_1\xi}{Q_0} & \frac{\nu\,k_2k_1}{Q_0} & 0 & 0 & \frac{Q_{11}}{Q_0} & 0 & 0 \\ \frac{k_4\nu\,\xi\,\alpha_1(1-\tau)}{bQ_0} & \frac{k_4\nu\,k_1\xi}{bQ_0} & \frac{k_4\nu\,k_2k_1}{bQ_0} & 0 & 0 & \frac{k_4Q_{12}}{bQ_0} & b^{-1} & 0 \\ \frac{Q_{13}\nu\,\xi\,\alpha_1(1-\tau)}{b\theta\,Q_0} & \frac{Q_{13}\nu\,k_1\xi}{b\theta\,Q_0} & \frac{Q_{13}\nu\,k_2k_1}{b\theta\,Q_0} & 0 & 0 & \frac{Q_{14}Q_{13}}{b\theta\,Q_0} & \frac{\eta_4}{b\theta} & \theta^{-1} \end{pmatrix},$$

where

$$\begin{aligned}
Q_0 &= k_5k_3k_2k_1 - k_5\xi\,\varphi\,k_1 - k_5\xi\,\alpha_1(1-\tau)f - \nu\,k_1\xi\,\alpha_2,\\
Q_1 &= -k_5\xi\,\varphi - \xi\,\alpha_2\nu + k_5k_3k_2,\\
Q_2 &= \varphi\,k_1k_5 + k_5\alpha_1f(1-\tau) + \nu\,k_1\alpha_2,\\
Q_3 &= \left((1-\tau)k_5\xi\,\alpha_1 + \alpha_1(1-\tau)k_5k_3 - k_5\xi\,\varphi - \xi\,\alpha_2\nu + k_5k_3k_2\right)k_4,\\
Q_4 &= k_5k_4\left(k_3k_1 + \xi\,k_1 + f\xi\right),\\
Q_5 &= \left(k_5\alpha_1f(1-\tau) + fk_2k_5 + k_2k_1k_5 + \varphi\,k_1k_5 + \nu\,k_1\alpha_2\right)k_4,\\
Q_6 &= k_4\alpha_2\left(k_3k_1 + \xi\,k_1 + f\xi\right),\\
Q_7 &= (1-\tau)k_5\alpha_1\left(\xi\,b\eta_5 + \xi\,\eta_3k_4 + \eta_3k_4k_3\right) - \left(\xi\,\varphi\,k_5 + \xi\,\alpha_2\nu - k_3k_2k_5\right)\left(\eta_1b + \eta_3k_4\right),\\
Q_8 &= k_5\left(\xi\,b\eta_5k_1 + \xi\,\eta_1bf + \eta_3k_4k_3k_1 + \xi\,\eta_3k_4k_1 + \xi\,\eta_3k_4f\right),\\
Q_9 &= \alpha_1\eta_3k_4k_5f(1-\tau) + fk_2b\eta_1k_5 + f\eta_3k_4k_2k_5 + \eta_3k_4\varphi\,k_1k_5 + \eta_3k_4k_2k_1k_5 + k_2b\eta_5k_1k_5 + \eta_3k_4\nu\,k_1\alpha_2,\\
Q_{10} &= \alpha_2\left(\xi\,b\eta_5k_1 + \xi\,b\eta_1f + \eta_3k_4k_3k_1 + \eta_3k_4\xi\,k_1 + \eta_3k_4\xi\,f\right),\\
Q_{11} &= k_3k_2k_1 - \xi\,\varphi\,k_1 - \xi\,\alpha_1(1-\tau)f,\\
Q_{12} &= k_3k_2k_1 - \xi\,\varphi\,k_1 - \xi\,\alpha_1(1-\tau)f,\\
Q_{13} &= \eta_2b + \eta_4k_4,\\
Q_{14} &= k_3k_2k_1 - \xi\,\varphi\,k_1 - \xi\,\alpha_1(1-\tau)f.
\end{aligned}$$

Then

$$J_{\mathcal{F}}J_{\mathcal{V}}^{-1} = \begin{pmatrix} k_{11} & Q_{15} & Q_{16} & Q_{17} & Q_{18} & k_{12} & 0 & 0 \\ 0 & 0 & 0 & 0 & 0 & 0 & 0 & 0 \\ 0 & 0 & 0 & 0 & 0 & 0 & 0 & 0 \\ 0 & 0 & 0 & 0 & 0 & 0 & 0 & 0 \\ 0 & 0 & 0 & 0 & 0 & 0 & 0 & 0 \\ k_{21} & Q_{19} & Q_{20} & 0 & 0 & k_{22} & Q_{21} & Q_{22} \\ 0 & 0 & 0 & 0 & 0 & 0 & 0 & 0 \\ 0 & 0 & 0 & 0 & 0 & 0 & 0 & 0 \end{pmatrix},$$

with

$$\begin{aligned}
k_{11} &= \frac{\beta_1 Q_1}{Q_0} + \frac{\beta_1\epsilon(1-\tau)\,\xi\,\alpha_1 k_5}{Q_0} + \frac{\beta_1\epsilon_1\Lambda_1 Q_3}{\mu\, bQ_0} + \frac{\beta_3\Lambda_1 Q_7}{\mu\, b\theta\, Q_0}, \\
k_{12} &= \frac{\beta_1 f\xi\,\alpha_2}{Q_0} + \frac{\beta_1\epsilon\,\xi\,\alpha_2 k_1}{Q_0} + \frac{\beta_1\epsilon_1\Lambda_1 Q_6}{\mu\, bQ_0} + \frac{\beta_3\Lambda_1 Q_{10}}{\mu\, b\theta\, Q_0}, \\
k_{21} &= \frac{\nu\,\xi\,\alpha_1(1-\tau)}{Q_0}\left(\beta_2\epsilon\, k_5 + \beta_2 + \frac{\beta_2\epsilon_2\Lambda_2 k_4}{\mu\, b} + \frac{\beta_3\Lambda_2 Q_{13}}{\mu\, b\theta}\right), \\
k_{22} &= \frac{\beta_2\epsilon\,\nu\,\xi\,\alpha_2 k_1}{Q_0} + \frac{\beta_2 Q_{11}}{Q_0} + \frac{\beta_2\epsilon_2\Lambda_2 k_4 Q_{12}}{\mu\, bQ_0} + \frac{\beta_3\Lambda_2 Q_{14} Q_{13}}{\mu\, b\theta\, Q_0}
\end{aligned}$$

$$\begin{aligned}
Q_{15} &= \frac{\beta_1 f k_5\xi}{Q_0} + \frac{\beta_1\epsilon\, k_1 k_5\xi}{Q_0} + \frac{\beta_1\epsilon_1\Lambda_1 Q_4}{\mu\, bQ_0} + \frac{\beta_3\Lambda_1 Q_8}{\mu\, b\theta\, Q_0}, \\
Q_{16} &= \frac{\beta_1 f k_2 k_5}{Q_0} + \frac{\beta_1\epsilon\, k_2 k_1 k_5}{Q_0} + \frac{\beta_1\epsilon_1\Lambda_1 Q_5}{\mu\, bQ_0} + \frac{\beta_3\Lambda_1 Q_9}{\mu\, b\theta\, Q_0}, \\
Q_{17} &= \frac{\beta_1\epsilon_1\Lambda_1}{\mu\, b} + \frac{\beta_3\Lambda_1\eta_3}{\mu\, b\theta}, \\
Q_{18} &= \frac{\beta_3\Lambda_1}{\mu\,\theta}, \\
Q_{19} &= \frac{\beta_2\epsilon\,\nu\, k_1 k_5\xi}{Q_0} + \frac{\beta_2\nu\, k_1\xi}{Q_0} + \frac{\beta_2\epsilon_2\Lambda_2 k_4\nu\, k_1\xi}{\mu\, bQ_0} + \frac{\beta_3\Lambda_2 Q_{13}\nu\, k_1\xi}{\mu\, b\theta\, Q_0}, \\
Q_{20} &= \frac{\beta_2\epsilon\,\nu\, k_2 k_1 k_5}{Q_0} + \frac{\beta_2\nu\, k_2 k_1}{Q_0} + \frac{\beta_2\epsilon_2\Lambda_2 k_4\nu\, k_2 k_1}{\mu\, bQ_0} + \frac{\beta_3\Lambda_2 Q_{13}\nu\, k_2 k_1}{\mu\, b\theta\, Q_0}, \\
Q_{21} &= \frac{\beta_2\epsilon_2\Lambda_2}{\mu\, b} + \frac{\beta_3\Lambda_2\eta_4}{\mu\, b\theta}, \\
Q_{22} &= \frac{\beta_3\Lambda_2}{\mu\,\theta}.
\end{aligned}$$

The potential non-vanishing eigenvalues of $J_{\mathcal{F}}J_{\mathcal{V}}^{-1}$ are those of the 2×2 matrix

$$\mathcal{K} = \begin{pmatrix} k_{11} & k_{12} \\ k_{21} & k_{22} \end{pmatrix}.$$

Therefore, the basic reproduction number is given by the spectral radius of $\mathcal{K}$ as follows:

$$\mathcal{R}_0 = \frac{k_{11} + k_{22} + \sqrt{(k_{11}-k_{22})^2 + 4\,k_{12}k_{21}}}{2}.$$

With this formula of $\mathcal{R}_0$, and using the baseline values of the parameters in Table 4 we obtain, $\mathcal{R}_0 = 2.95$, which, in view of conflicts and war, is slightly higher than other reported values (Legrand et al. 2007, Berge et al. 2017c). In the numerical simulations' section, other estimations of $\mathcal{R}_0$ will be obtained by varying the parameters within the ranges provided in Table 4.

Remark 4.2. *A follow-up to Remark 2.1 is in order with regard to the hospital destruction parameter τ and the associated movement parameters ν, f and φ due to patient escape at the rate ξ. If $\tau = 1$ and $\nu = 0$ such that there is no transmission of the EVD in Patch 2 coming from Patch 1, then $\mathcal{R}_0$ reduces to the basic reproduction for Patch 1 sub-model. However, if $0 \leq \tau < 1$ and $\nu > 0$ so that the two patches are coupled, then infectious individuals from Patch 2 will be admitted in hospital in Patch 1 at the rate α_2. We emphasize that the rate is indeed α_2 and not $\alpha_2(1-\tau)$ because escaped patients and those infected by them are priority and urgent cases for admission in the operational ETCs. Note that the case when $\nu > 0$ makes the disease more severe in the sense that, as function of ν, the basic reproduction number satisfies the relation $\mathcal{R}_0(\nu) > \mathcal{R}_0(0)$, since it can be shown that $k_{22}(\nu) > k_{22}(0)$.*

The stability result stated below follows from Theorem 2 in (Van den Driessche & Watmough 2002).

Theorem 4.3. *The Disease-free equilibrium point E_0 of the model (6)-(7) is locally asymptotically stable (LAS) if $\mathcal{R}_0 < 1$ and unstable whenever $\mathcal{R}_0 > 1$.*

The threshold theory contained in Theorem 4.3 can be paraphrased in the following epidemiological terms: a small influx of EVD infectious into a community of susceptible individuals will not generate large EVD outbreaks unless the number of susceptibles is above a certain critical values; in other words, the EVD eventually dies out when the basic reproduction number is less than unity. To ensure that the EVD elimination is independent of the initial sizes of the dependent variables, we have the next result that improves Theorem 4.3.

Theorem 4.4. *The disease-free equilibrium E_0 of the model (6)-(7) is globally asymptotically stable (GAS) whenever $\mathcal{R}_0 < 1$.*

Proof: We use a theorem on page 246 in (Castillo-Chavez et al. 2002), which we state in a relatively self-contained manner given our intention to extend it to discrete dynamical systems in the next section. To this end, we re-write the system (6)-(7) in the framework of the said theorem as follows:

$$\frac{dX}{dt} = F(X, Y), \tag{24}$$

$$\frac{dY}{dt} = G(X, Y) \text{ with } G(X, 0) = 0. \tag{25}$$

Here, $X = (S_1, R_1, S_2, R_2) \in \mathbb{R}^4_+$ and $Y = (I_1, H, L, D_1, P_1, I_2, D_2, P_2) \in \mathbb{R}^8_+$ denote the dependent variables of uninfected and infected individuals, respectively; the right hand sides

are

$$F(X,Y)=\begin{pmatrix}\Lambda_1-(\lambda_1+\mu)S_1\\ \gamma_1 I_1+\gamma_3 H-\mu R_1\\ \Lambda_2-(\lambda_2+\mu)S_2\\ \gamma_2 I_2-\mu R_2\end{pmatrix}\quad\text{and}\quad G(X,Y)=\begin{pmatrix}\lambda_1 S_1+fL-k_1 I_1\\ \alpha_1(1-\tau)I_1+\alpha_2 I_2+\varphi L-k_2 H\\ \xi H-k_3 L\\ k_4(I_1+H+L)-bD_1\\ \eta_1 I_1+\eta_3 D_1+\eta_5 L-\theta P_1\\ \lambda_2 S_2+\nu L-k_5 I_2\\ k_4 I_2-bD_2\\ \eta_2 I_2+\eta_4 D_2-\theta P_2,\end{pmatrix}$$

According to theorem in (Castillo-Chavez et al. 2002), the disease-free equilibrium in (22) in this setting can be written as

$$E_0\equiv(X^*,0)=\left(\frac{\Lambda_1}{\mu},0,\frac{\Lambda_2}{\mu},0,0,0,0,0,0,0,0,0\right)$$

is globally asymptotically stable for $\mathcal{R}_0<1$ provided that the following conditions are satisfied for $(X,Y)\in\Omega$:

(H1) For the sub-system $\dfrac{dX}{dt}=F(X,0)$, the equilibrium point, $X^*=\left(\frac{\Lambda_1}{\mu},0,\frac{\Lambda_2}{\mu},0\right)$, is globally asymptotically stable.

(H2) The right-hand side of Eq (25) admits the decomposition

$$G(X,Y)=AY-\tilde{G}(X,Y)$$

where $\tilde{G}(X,Y)\geq 0$ and A, the Jacobian matrix of $G(X,Y)$ with respect to Y at E_0, is an Metzler matrix (the off diagonal elements of A are nonnegative).

With $F(X,0)=(\Lambda_1-\mu S_1,-\mu R_1,\Lambda_2-\mu S_2,-\mu R_2)^T$, the condition (H1) is clearly satisfied for this decoupled linear system. As per the condition (H2), we observe that the Jacobian matrix given by

$$A=\begin{pmatrix}\beta_1-k_1 & 0 & \beta_1\epsilon+f & \beta_1\frac{\epsilon_1\Lambda_1}{\mu} & \beta_3\frac{\Lambda_1}{\mu} & 0 & 0 & 0\\ \alpha_1(1-\tau) & -k_2 & \varphi & 0 & 0 & \alpha_2 & 0 & 0\\ 0 & \xi & -k_3 & 0 & 0 & 0 & 0 & 0\\ k_4 & k_4 & k_4 & -b & 0 & 0 & 0 & 0\\ \eta_1 & 0 & \eta_5 & \eta_3 & -\theta & 0 & 0 & 0\\ 0 & 0 & \beta_2\epsilon\nu+\nu & 0 & 0 & \beta_2-k_5 & \beta_2\frac{\epsilon_2\Lambda_2}{\mu} & \beta_3\frac{\Lambda_2}{\mu}\\ 0 & 0 & 0 & 0 & 0 & k_4 & -b & 0\\ 0 & 0 & 0 & 0 & 0 & \eta_2 & \eta_4 & -\theta\end{pmatrix}$$

is clearly an Metzler-matrix. Finally, for $(X, Y) \in \Omega$, the required decomposition is realized with

$$\begin{aligned}
\tilde{G}(X,Y) &= \begin{pmatrix} -\lambda_1 S_1 + \beta_1 I_1 + \beta_1 \epsilon L + \beta_1 \frac{\epsilon_1 \Lambda_1}{\mu} D_1 + \beta_3 \frac{\Lambda_1}{\mu} P_1 \\ 0 \\ 0 \\ 0 \\ 0 \\ -\lambda_2 S_2 + \beta_2 \epsilon \nu L + \beta_2 I_2 + \beta_2 \frac{\epsilon_2 \Lambda_2}{\mu} D_2 + \beta_3 \frac{\Lambda_2}{\mu} P_2 \\ 0 \\ 0 \\ 0 \end{pmatrix} \\
&= \begin{pmatrix} \beta_1 \left(1 - \frac{S_1}{N_1}\right)(I_1 + \epsilon L) + \left(\frac{\Lambda_1}{\mu} - S_1\right)(\beta_1 \epsilon_1 D_1 + \beta_3 P_1) \\ 0 \\ 0 \\ 0 \\ 0 \\ \beta_2 \left(1 - \frac{S_2}{N_2 + \nu L}\right)(I_2 + \epsilon \nu L) + \left(\frac{\Lambda_2}{\mu} - S_2\right)(\beta_2 \epsilon_2 D_2 + \beta_3 P_2) \\ 0 \\ 0 \\ 0 \end{pmatrix} \\
&\geq 0,
\end{aligned}$$

where the expressions of the forces of infection λ_i in (4) and (5) and the definition of the region Ω were used in the previous two relations. This completes the proof of Theorem 4.4. □

Remark 4.5. *The method used to prove Theorem 4.4 does not lead to a conclusion for the stability of E_0 when $\mathcal{R}_0 = 1$. Typically, this is investigated by constructing a Lyapunov function and applying the LaSalle's Invariance Principle (La Salle 1976). In the current situation, the expression of the basic reproduction number $\mathcal{R}_0$ is complicated and highly nonlinear with respect to its coefficients, which makes it difficult to use it directly. To avoid such difficulty, specifically in the context of patch-models, it is standard to use an alternative threshold quantity (see, for instance (Tsanou et al. 2017a)). For the case under consideration, one can use the quantity $\mathcal{T}_0 := \dfrac{k_{11} + k_{22} + k_{12}k_{21}}{1 + k_{11}k_{22}}$, which has the following properties:*

$$\textit{If } k_{11} + k_{22} \geq 2, \textit{ then } \mathcal{R}_0 > 1. \textit{ If } k_{11} + k_{22} < 2, \textit{ then } \mathcal{R}_0 \leq (\geq) 1 \Longleftrightarrow \mathcal{T}_0 \leq (\geq) 1.$$

The above relation between the thresholds $\mathcal{R}_0$ and $\mathcal{T}_0$ is illustrated on Figure 5 where they are plotted against the parameter ν that accounts for the worst scenario on the movement of patients who escape from hospitals, namely moving to Patch 2 where there are no control measures. When the two thresholds are less than one, $\mathcal{T}_0$ always dominates $\mathcal{R}_0$ so that it is

better to use $\mathcal{R}_0$ for the control of the disease in this case. However, the use of $\mathcal{T}_0$ could be appropriate when both $\mathcal{R}_0$ and $\mathcal{T}_0$ are greater than one, since $\mathcal{R}_0 > \mathcal{T}_0$. Anyway, despite the introduction of the threshold quantity $\mathcal{T}_0$, the proof of the GAS of E_0 for $\mathcal{R}_0 = 1$ remains a difficult question, which is not the focus of this work.

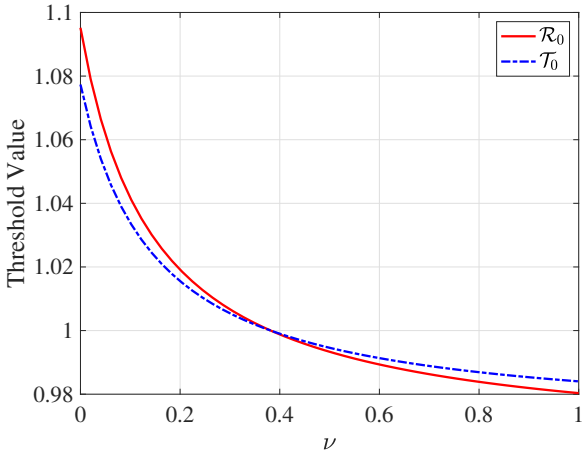

Figure 5: Comparison of threshold quantities $\mathcal{R}_0$ and $\mathcal{T}_0$. The parameters are chosen based on baseline values in Table 4 with the following adjustments: $\beta_1 = 6.150\times10^{-3}$, $\beta_2 = 1.994\times10^{-3}$, and $\beta_3 = 1.161\times10^{-3}$.

Having studied the disease-free equilibrium E_0 of the model (6)-(7), we now investigate its potential endemic equilibria (EE), *i.e.* solutions of the algebraic system (21) with at least some positive infected classes, which are denoted

$$E^* = (S_1^*, I_1^*, H^*, L^*, R_1^*, D_1^*, P_1^*, S_2^*, I_2^*, R_2^*, D_2^*, P_2^*). \tag{26}$$

We start with an interior EE whereby all the infective coordinates I_1^*, H^*, L^*, D_1^*, P_1^*, I_2^*, D_2^* and P_2^* are positive. Then after further simplifications in the defining relation (21), we obtain

$$\begin{aligned}
S_1^* &= \frac{\Lambda_1}{\lambda_1^*+\mu}, \quad I_1^* = \frac{1}{k_1}\left(\frac{\Lambda_1\lambda_1^*}{\lambda_1^*+\mu} + fL^*\right), \quad H^* = \frac{k_3}{\xi}L^*, \quad R_1^* = \frac{\gamma_1}{\mu k_1}\frac{\Lambda_1\lambda_1^*}{(\lambda_1^*+\mu)} + x_1L^*,\\
D_1^* &= \frac{k_4\Lambda_1\lambda_1^*}{bk_1(\lambda_1^*+\mu)} + x_2L^*, \quad P_1^* = \frac{x_3\lambda_1^*}{\lambda_1^*+\mu} + \frac{1}{\theta}\left(\frac{\eta_1 f}{k_1} + \eta_3x_2 + \eta_5\right)L^*,\\
S_2^* &= \frac{\Lambda_2}{\lambda_2^*+\mu}, \quad I_2^* = \frac{1}{k_5}\left(\frac{\Lambda_2\lambda_2^*}{\lambda_2^*+\mu} + \nu L^*\right), \quad R_2^* = \frac{\gamma_2}{\mu k_5}\left(\frac{\Lambda_2\lambda_2^*}{\lambda_2^*+\mu} + \nu L^*\right),\\
D_2^* &= \frac{k_4}{bk_5}\left(\frac{\Lambda_2\lambda_2^*}{\lambda_2^*+\mu} + \nu L^*\right), \quad P_2^* = \frac{x_4\lambda_2^*}{\lambda_2^*+\mu} + \frac{1}{\theta}\left(\frac{\eta_2\nu}{k_5} + \frac{\eta_4k_4\nu}{bk_5}\right)L^*,
\end{aligned} \tag{27}$$

where $\lambda_1^* \equiv \lambda_1^*(E^*)$ and $\lambda_2^* \equiv \lambda_2^*(E^*)$ denote the forces of infection in (4) and (5) evaluated at E^*, while

$$x_1 = \frac{1}{\mu}\left(f + \frac{\gamma_3k_3}{\xi}\right), \; x_2 = \frac{k_4}{b}\left(\frac{f}{k_1} + \frac{k_3}{\xi} + 1\right),$$
$$x_3 = \frac{\Lambda_1}{\theta}\left(\frac{\eta_1}{k_1} + \frac{\eta_3k_4}{bk_1}\right) \quad \text{and} \quad x_4 = \frac{\Lambda_2}{\theta}\left(\frac{\eta_2}{k_5} + \frac{\eta_4k_4}{bk_5}\right).$$

Given the strong nonlinearity of the model already mentioned in Remark 4.5 and displayed now in (27) as well as in the complex expressions of $\lambda_1^*(E^*)$ and $\lambda_2^*(E^*)$, it is clear that establishing the existence of interior equilibria is a challenging task. Therefore, we will address this question later on numerical simulations. In the meantime, it is worthy to investigate the existence of boundary endemic equilibria as explained below.

We assume that $\nu > 0$ so that the patches are coupled. We look for a Patch 1 boundary equilibrium or Patch 2 disease-free equilibrium in the sense that $I_2 = D_2 = P_2 = 0$, but all the coordinates I_1, D_1 and P_1 are positive in E^*. With the requirement $I_2^* = 0$, it follows from the implicit expression, (27), of a solution of the system (21) that $\lambda_2^* = 0$ and $L^* = 0$. Hence, we obtain a boundary equilibrium

$$\begin{aligned} E^* &= (S_1^*, I_1^*, H^*, L^*, R_1^*, D_1^*, P_1^*, S_2^*, I_2^*, R_2^*, D_2^*, P_2^*) \\ &= \left(\frac{\Lambda_1}{\lambda_1^* + \mu}, \frac{\lambda_1^* S_1^*}{k_1}, 0, 0, \frac{\gamma_1 I_1^*}{\mu}, \frac{(\mu+\delta) I_1^*}{b}, \frac{\eta_1 I_1^* + \eta_3 D_1^*}{\theta}, \frac{\Lambda_2}{\mu}, 0, 0, 0, 0 \right). \end{aligned} \tag{28}$$

In a similar manner, there is a Patch 2 boundary equilibrium or Patch 1 disease-free equilibrium given by

$$\begin{aligned} E^* &= (S_1^*, I_1^*, H^*, L^*, R_1^*, D_1^*, P_1^*, S_2^*, I_2^*, R_2^*, D_2^*, P_2^*) \\ &= \left(\frac{\Lambda_1}{\mu}, 0, 0, 0, 0, 0, 0, \frac{\Lambda_2}{\lambda_2^* + \mu}, \frac{\Lambda_2 \lambda_2^*}{k_5(\lambda_2^* + \mu)}, \frac{\gamma_2 \Lambda_2 \lambda_2^*}{\mu k_5(\lambda_2^* + \mu)}, \frac{k_4 \Lambda_2 \lambda_2^*}{b k_5(\lambda_2^* + \mu)}, \frac{x_4 \lambda_2^*}{\lambda_2^* + \mu} \right). \end{aligned} \tag{29}$$

We have the following result:

Theorem 4.6. *Under the condition $\nu > 0$, the model (6)-(7) has at least one Patch 1 boundary equilibrium and Patch 2 boundary equilibrium, which are given by (28) and (29) and are locally asymptotically stable whenever $\mathcal{R}_0 > 1$ is close to 1.*

Proof: We give the proof for the Patch 1 boundary equilibrium, the situation being similar for the other boundary equilibrium. By combining Eq. (28) with $\lambda_1^* \equiv \lambda_1^*(E^*)$ given in Eq. (4), and by doing some algebraic manipulations, we obtain the following third degree polynomial in λ_1^*:

$$\lambda_1^* \left(K_2 (\lambda_1^*)^2 + K_1 \lambda_1^* + K_0 \right) = 0. \tag{30}$$

Here

$$\begin{aligned} K_2 &= b(\gamma_1 + \mu + \delta)(\mu + \gamma_1), \\ K_1 &= \mu(\gamma_1 + \mu + \delta)^2 b + x_6(\mu + \gamma_1) - \mu(\gamma_1 + \mu + \delta) b \beta_1, \\ K_0 &= (x_6 - b\beta_1)\mu(\gamma_1 + \mu + \delta), \\ &= b\mu^2(\gamma_1 + \mu + \delta)^2 (1 - \mathcal{R}_0), \end{aligned}$$

where $x_6 = \mu b(\gamma_1 + \mu + \delta) - \beta_1 \epsilon_1 k_4 \Lambda_1 - b(\gamma_1 + \mu + \delta)\beta_3 x_3$. The previous relation that involves $\mathcal{R}_0$ in its reduced form below, due to the Patch 2 disease-free equilibrium, is obtained after

further simplification:

$$\mathcal{R}_0 = \frac{\beta_1}{k_1}\left(1 + \frac{\epsilon_1 \Lambda_1 k_4}{\mu b}\right) + \frac{\beta_3 \Lambda_1 k_3}{\mu \theta k_1 k_5}\left(\eta_1 + \frac{\eta_3 k_4}{b}\right).$$

Clearly, $\lambda_1^* = 0$ gives the disease-free equilibrium E_0 in Eq. (22), with $P_1 = P_2 = 0$. We therefore consider the quadratic polynomial,

$$K_2(\lambda_1^*)^2 + K_1\lambda_1^* + K_0 = 0, \tag{31}$$

whose possible sign changes of coefficients depend on K_1 and K_0 given that $K_2 > 0$. This is summarized in the following table.

No.	Sign of K_1	Sign of K_0	Number of possible root(s)
1	+	+	No root
2	+	-	one root
3	-	-	one root

Table 5: Existence of Patch 1 boundary equilibrium

When $\mathcal{R}_0 > 1$, it follows from the table (no 2 or 3) and Descarte's rule of signs that there exists a unique EE. The local asymptotic stability of this endemic equilibrium for $\mathcal{R}_0 > 1$ close to 1 is guaranteed by the Center Manifold Theorem in (Castillo-Chavez & Song 2004). (Note that the scenario no. 1 in the table corresponds to the case when $\mathcal{R}_0 < 1$ and is in agreement with Theorem 4.4, which implies that there is no EE). This completes the proof. □

5 Nonstandard finite difference scheme

The nonstandard finite difference (NSFD) method was initiated more than three decades ago by Mickens. Paraphrasing him from his latest book (Mickens 2020), the NSFD method is becoming an established field whose the concept of dynamic consistency and associated techniques are increasingly and quickly accepted for the construction of reliable numerical schemes for differential equations. In this section, we construct a NSFD scheme that replicates the dynamics of the EVD model (6)-(7).

Let

$$Z^k = \left(S_1^k, I_1^k, H^k, L^k, R_1^k, D_1^k, P_1^k, S_2^k, I_2^k, R_2^k, D_2^k, P_2^k\right)^T$$

denote an approximation of

$$Z(t_k) = (S_1(t_k), I_1(t_k), H(t_k), L(t_k), R_1(t_k), D_1(t_k), P_1(t_k), S_2(t_k), I_2(t_k), R_2(t_k), D_2(t_k), P_2(t_k))^T$$

at the time $t_k = k\triangle t$, $k \in \mathbb{N}$, where $h = \triangle t > 0$ is the step size. Following the methodology in (Anguelov & Lubuma 2001, Anguelov et al. 2014, Mickens 1994), as revisited in (Anguelov

et al. 2020, Mickens 2020) for some infectious disease models, we propose the following NSFD scheme:

$$\begin{cases} \dfrac{S_1^{k+1}-S_1^k}{\phi} = \Lambda_1 - (\lambda_1^k + \mu)S_1^{k+1}, \\ \dfrac{I_1^{k+1}-I_1^k}{\phi} = \lambda_1^k S_1^{k+1} + fL^k - k_1 I_1^{k+1}, \\ \dfrac{H^{k+1}-H^k}{\phi} = \alpha_1(1-\tau)I_1^{k+1} + \alpha_2 I_2^k + \varphi L^k - k_2 H^{k+1}, \\ \dfrac{L^{k+1}-L^k}{\phi} = \xi H^{k+1} - k_3 L^{k+1}, \\ \dfrac{R_1^{k+1}-R_1^k}{\phi} = \gamma_1 I_1^{k+1} + \gamma_3 H^{k+1} - \mu R_1^{k+1}, \\ \dfrac{D_1^{k+1}-D_1^k}{\phi} = k_4(I_1^{k+1} + H^{k+1} + L^{k+1}) - bD_1^{k+1}, \\ \dfrac{P_1^{k+1}-P_1^k}{\phi} = \eta_1 I_1^k + \eta_3 D_1^k + \eta_5 L^k - \theta P_1^{k+1}. \end{cases} \tag{32}$$

$$\begin{cases} \dfrac{S_2^{k+1}-S_2^k}{\phi} = \Lambda_2 - (\lambda_2^k + \mu)S_2^{k+1}, \\ \dfrac{I_2^{k+1}-I_2^k}{\phi} = \lambda_2^k S_2^{k+1} + \nu L^{k+1} - k_5 I_2^{k+1}, \\ \dfrac{R_2^{k+1}-R_2^k}{\phi} = \gamma_2 I_2^{k+1} - \mu R_2^{k+1}, \\ \dfrac{D_2^{k+1}-D_2^k}{\phi} = k_4 I_2^{k+1} - bD_2^{k+1}, \\ \dfrac{P_2^{k+1}-P_2^k}{\phi} = \eta_2 I_2^k + \eta_4 D_2^k - \theta P_2^{k+1}. \end{cases} \tag{33}$$

In (32)-(33), the denominator function $\phi = \phi(h)$ that satisfies the relation $\phi(h) = h + \mathcal{O}(h^2)$ is defined by

$$\phi = \phi(h) = \frac{1 - e^{-qh}}{q} \tag{34}$$

where the number $q > 0$ is large enough so that it captures the qualitative feature of the model (6)-(7). Typically, as explained in (Anguelov et al. 2020), one can take

$$q \geq (\mu + \alpha_1 + \alpha_2 + \gamma_1 + \gamma_2 + \gamma_3 + \delta + \xi + f + \varphi + \nu + b + \theta). \tag{35}$$

Note that some of the parameters could be excluded from (35), *e.g.*, the rate b of deceased human individuals who are not directly buried because this number is supposed to be less than or equal to the disease-induced death rate δ that is included in the expression. But, we have included all the parameters to simplify the presentation. Furthermore, other qualitative parameters such as the eigenvalues of underlying Jacobian matrices will be added in the right-hand of Eq. (35). The forces of infection are discretized as follows to re-inforce Mickens' rule on nonlocal approximation of nonlinear terms:

$$\lambda_1^k = \beta_1 \left(\frac{I_1^k + \epsilon L^k}{N_1^k} + \epsilon_1 D_1^k \right) + \beta_3 P_1^k \text{ and } \lambda_2^k = \beta_2 \left(\frac{I_2^k + \epsilon\nu L^k}{N_2^k + \nu L^k} + \epsilon_2 D_2^k \right) + \beta_3 P_2^k \tag{36}$$

where $N^k = N_1^k + N_2^k$, $N_1^k = S_1^k + I_1^k + H^k + L^k + R_1^k$ and $N_2^k = S_2^k + I_2^k + R_2^k$.

Remark 5.1. *Occasionally, we will use the simplest explicit NSFD scheme, namely the nonstandard forward Euler scheme defined by considering all the discretizations in the right-hand sides of (32)-(32) to be local at the time t_k; see, for instance, (Anguelov & Lubuma 2001, Mickens 1994).*

The NSFD scheme (32)-(33) is equivalent to the formulation (37)-(38) below in the Gauss-Seidel order, which is suitable for computational purpose.

$$\begin{cases} S_1^{k+1} = \dfrac{\Lambda_1\phi + S_1^k}{1 + (\lambda_1^k + \mu)\phi}, & I_1^{k+1} = \dfrac{\left(\lambda_1^k S_1^{k+1} + fL^k\right)\phi + I_1^k}{1 + k_1\phi} \\ H^{k+1} = \dfrac{\left(\alpha_1(1-\tau)I_1^{k+1} + \alpha_2 I_2^k + \varphi L^k\right)\phi + H^k}{1 + k_2\phi}, & L^{k+1} = \dfrac{\xi H^{k+1}\phi + L^k}{1 + k_3\phi}, \\ R_1^{k+1} = \dfrac{\left(\gamma_1 I_1^{k+1} + \gamma_3 H^{k+1}\right)\phi + R_1^K}{1 + \mu\phi} & D_1^{k+1} = \dfrac{k_4\left(I_1^{k+1} + H^{k+1} + L^{k+1}\right)\phi + D_1^k}{1 + b\phi}, \\ P_1^{k+1} = \dfrac{\left(\eta_1 I_1^k + \eta_3 D_1^k + \eta_5 L^k\right)\phi + P_1^k}{1 + \theta\phi} \end{cases} \tag{37}$$

$$\begin{cases} S_2^{k+1} = \dfrac{\Lambda_2\phi + S_2^k}{1 + (\lambda_2^k + \mu)\phi}, & I_2^{k+1} = \dfrac{\left(\lambda_2^k S_2^{k+1} + \nu L^k\right)\phi + I_2^k}{1 + k_5\phi}, \\ R_2^{k+1} = \dfrac{\gamma_2 I_2^{k+1}\phi + R_2^k}{1 + \mu\phi}, & D_2^{k+1} = \dfrac{k_4 I_2^{k+1}\phi + D_2^k}{1 + b\phi}, \\ P_2^{k+1} = \dfrac{\left(\eta_2 I_2^k + \eta_4 D_2^k\right)\phi + P_2^k}{1 + \theta\phi}. \end{cases} \tag{38}$$

By implementing the discrete analogue of the reasoning in the proof of Theorem 4.1, as done in (Anguelov et al. 2020), we obtain the following result:

Theorem 5.2. *The NSFD scheme (32)-(33) or (37)-(38) is dynamically consistent with respect to Theorem 4.1 in the sense that this scheme is a discrete dynamical system on the same biologically feasible region Ω, which is equally attracting.*

It is clear that as discrete dynamical systems, the NSFD scheme (32)-(33) or (37)-(38) as well as the nonstandard Euler scheme mentioned in Remark 5.1 have the unique disease-free fixed (DFF) point,

$$\text{DFF} \equiv E_0 = \left(\frac{\Lambda_1}{\mu}, 0, 0, 0, 0, 0, 0, \frac{\Lambda_2}{\mu}, 0, 0, 0, 0\right), \tag{39}$$

which turns out to be the unique disease-free equilibrium (DFE) point in (22) of the continuous model (6)-(7). In order to study the stability of the DFF point, we state a theorem, which is a discrete analogue of the result used in the proof of Theorem 4.4 to prove the global asymptotic stability of the DFE point of the system (6)-(7) re-written in the form (24)-(25).

Theorem 5.3. *Let us consider a discrete dynamical system on* $\Omega \subset \mathbb{R}^m_+ \times \mathbb{R}^n_+$ *of the form*

$$\begin{cases} X^{k+1} = F_h(X^k, Y^k), \\ Y^{k+1} = G_h(X^k, Y^k), \qquad G_h(X^k, 0) = 0. \end{cases} \tag{40}$$

We assume that the system has a unique fixed-point $Z^* = (X^*, 0)$, $X^* > 0$, *which is stable. We further assume that*

$(\mathcal{D}_1)$ *For the sub-system* $X^{k+1} = F_h(X^k, 0)$, *the fixed-point point* X^* *is globally asymptotically stable;*

$(\mathcal{D}_2)$ *The right-hand side of the second equation of the discrete dynamical system on* Ω, *(40), admits the decomposition*

$$G_h(X^k, Y^k) = A_h Y^k - \tilde{G}_h(X^k, Y^k),$$

where $\tilde{G}_h(X^k, Y^k) \geq 0$ *and* A_h *is a Metzler matrix with spectral radius,* $\rho(A_h) < 1$.

Then, the fixed-point $(X^*, 0)$ *is globally asymptotically stable on* Ω.

Proof: Let $\{(X^k, Y^k)\}_k$ be the sequence in Ω generated by (40) from an arbitrary initial guess $(X^0, Y^0) \in \Omega$. By mathematical induction, the second equation in (40) and Condition $(\mathcal{D}_2)$ lead to

$$0 \leq Y^k \leq (A_h)^k Y^0. \tag{41}$$

Since $\rho(A_h) < 1$, the sequence of matrices $\{A_h^k\}_k$ converges to the zero matrix, and thus $Y^k \to 0$ as $k \to \infty$. Combining this with Condition $(\mathcal{D}_1)$, it follows that the fixed-point $(X^*, 0)$ is attractive and, thus, globally asymptotically stable because it was assumed to be stable.

Theorem 5.4. *The disease-free fixed point (39) of the nonstandard Euler scheme referred to in Remark 5.1 is globally asymptotically stable whenever* $\mathcal{R}_0 < 1$, *and* q *is suitably chosen.*

Proof: By a suitable choice of the parameter q in (34)-(35), it can be shown, as done elsewhere (*e.g.* (Anguelov et al. 2020, 2014)), that the nonstandard Euler scheme is elementary stable. In particular, when $\mathcal{R}_0 < 1$, the disease-free equilibrium point (DFE), E_0, is the unique fixed-point of the discrete dynamical system and it is locally asymptotically stable.

Next, we use the notation $X^k = (S_1^k, R_1^k, S_2^k, R_2^k)$ and $Y^k = (I_1^k, H^k, L^k, D_1^k, P_1^k, I_2^k, D_2^k, P_2^k)$ for the respective uninfected and infected classes, and we apply Theorem 5.3. The nonstandard Euler scheme can be written in the form (40), with vector functions $F_h \equiv F_h(X^k, Y^k) : \mathbb{R}^4 \times \mathbb{R}^4 \to \mathbb{R}^4$ and $G_h \equiv G_h(X^k, Y^k) : \mathbb{R}^8 \times \mathbb{R}^8 \to \mathbb{R}^8$ given as follows in terms of the functions F and G in the continuous model (24)-(25):

$$F_h(X^k, Y^k) = X^k + \phi F(X^k, Y^k) \text{ and } G_h(X^k, Y^k) = Y^k + \phi G(X^k, Y^k), \text{ with } G_h(X^k, 0) = 0. \tag{42}$$

It is readily seen that the sub-system referred to in Condition (D_1) of Theorem 5.3 is the following system of four first order difference equations:

$$X^{k+1} = F_h(X^k, 0) = \begin{pmatrix} \phi\Lambda_1 + S_1^k(1 - \phi\mu) \\ 0 \\ \phi\Lambda_2 + S_2^k(1 - \phi\mu) \\ 0 \end{pmatrix} = \begin{pmatrix} \phi\Lambda_1 \displaystyle\sum_{j=0}^{k} (1 - \phi\mu)^j + (1 - \phi\mu)^{k+1} S_{01} \\ 0 \\ \phi\Lambda_2 \displaystyle\sum_{j=0}^{k} (1 - \phi\mu)^j + (1 - \phi\mu)^{k+1} S_{02} \\ 0 \end{pmatrix}.$$

Consequently, the sequence $\{X^k\}_k$ converges to the fixed-point $X^* = \left(\frac{\Lambda_1}{\mu}, 0, \frac{\Lambda_2}{\mu}, 0\right)$ as $k \to \infty$. Hence, X^* is globally asymptotically stable, as needed from Condition (D_1).

Regarding Condition $(\mathcal{D}_2)$, we observe that the function G_h in (42) admits the required decomposition with $\tilde{G}_h(X^k, Y^k) = \phi\tilde{G}(X^k, Y^k) \geq 0$ and $A_h = I + \phi A$ where $\tilde{G}$ and A are the same vector function and Metzler matrix that were used in Condition (H_2) in the proof of Theorem 4.4 for the continuous model. Given this relation between the discrete and the continuous matrices, any eigenvalue λ_h of A_h corresponds to an eigenvalue λ of A through the relation $\lambda_h = 1 + \phi\lambda$. When $\mathcal{R}_0 < 1$, we have $\Re\lambda = -|\Re\lambda| < 0$, so that $|\lambda_h|^2 = 1 - 2\phi|\Re\lambda| + \phi^2|\lambda|^2$. Thus $|\lambda_h| < 1$ whenever $\phi < 2|\Re\lambda|/|\lambda|^2$, which leads to the requirement $q \geq |\lambda|^2|/2|\Re\lambda|$, $\forall\lambda$, for the spectral radius of A_h to be less than 1. Hence the sequence $\{Y^k\}_k$ converges to 0. Thus the DFF, E_0, is globally asymptotically stable. This completes the proof of the theorem. □

Remark 5.5. *In terms of the first equation of the structure (40), the NSFD scheme (32)-(33) or (37)-(38), can be written as*

$$X^{k+1} = F_h \equiv \begin{pmatrix} \frac{\Lambda_1\phi + S_1^k}{1+(\lambda_1^k+\mu)\phi} \\ \frac{1}{1+\mu\phi}\left\{\left(\gamma_1 + \frac{\alpha_1\gamma_3(1-\tau)}{1+k_2\phi}\right)\frac{1}{1+k_1\phi}\left[\left(\frac{\lambda_1^k(\Lambda_1\phi+S_1^k)}{1+(\lambda_1^k+\mu)\phi} + fL^k\right)\phi + I_1^k\right] + \frac{\gamma_3\left((\alpha_2 I_2^k + \varphi L^k)\phi + H^k\right)\phi}{1+k_2\phi} + R_1^k\right\} \\ \frac{\Lambda_2\phi + S_2^k}{1+(\lambda_2^k+\mu)\phi} \\ \frac{1}{1+\mu\phi}\left\{\frac{\gamma_2}{1+k_5\phi}\left[\left(\frac{\lambda_2^k(\Lambda_2\phi+S_2^k)}{1+(\lambda_2^k+\mu)\phi} + \nu L^k\right)\phi + I_2^k\right]\phi + R_2^k\right\} \end{pmatrix}. \tag{43}$$

Hence, the fixed-point $X^* = \left(\frac{\Lambda_1}{\mu}, 0, \frac{\Lambda_2}{\mu}, 0\right)$ *is, as needed from Condition* $(\mathcal{D}_2)$*, globally asymptotically stable for the following sub-system:*

$$X^{k+1} = F_h(X^k, 0) = \begin{pmatrix} \frac{\Lambda_1\phi + S_1^k}{1+\mu\phi} \\ 0 \\ \frac{\Lambda_2\phi + S_2^k}{1+\mu\phi} \\ 0 \end{pmatrix} = \begin{pmatrix} \frac{\Lambda_1}{\mu} + \left(S_{01} - \frac{\Lambda_1}{\mu}\right)\left(\frac{1}{1+\mu\phi}\right)^k \\ 0 \\ \frac{\Lambda_2}{\mu} + \left(S_{02} - \frac{\Lambda_2}{\mu}\right)\left(\frac{1}{1+\mu\phi}\right)^k \\ 0 \end{pmatrix}.$$

For the second equation in (40), we obtain

$$7Y^{k+1} = G_h \equiv \begin{pmatrix} \frac{1}{1+k_1\phi}\left((T_1^k + fL^k)\phi + I_1^k\right) \\ \frac{1}{1+k_2\phi}\left\{\left[\frac{\alpha_1(1-\tau)}{1+k_1\phi}\left((T_1^k + fL^k)\phi + I_1^k\right) + \alpha_2 I_2^k + \varphi L^k\right]\phi + H^k\right\} \\ \frac{1}{1+k_3\phi}\left\{\frac{\xi}{1+k_2\phi}\left\{\left[\frac{\alpha_1(1-\tau)}{1+k_1\phi}\left((T_1^k + fL^k)\phi + I_1^k\right) + \alpha_2 I_2^k + \varphi L^k\right]\phi + H^k\right\}\phi + L^k\right\} \\ \frac{\mu+\delta}{1+\mu\phi}\left\{\left[\left((T_1^k + fL^k)\phi + I_1^k\right) + T_3 I_2^k + T_4 L^k + T_5 H^k\right]\phi + D_1^k\right\} \\ \frac{1}{1+\theta\phi}\left[(\eta_1 I_1^k + \eta_3 D_1^k + \eta_5 L^k)\phi + P_1^k\right] \\ \frac{1}{1+k_5\phi}\left((Z^k + \nu L^k)\phi + I_2^k\right) \\ \frac{1}{1+b\phi}\left[\frac{k_4}{1+k_5\phi}\left[(Z^k + \nu L^k)\phi + I_2^k\right)\phi + D_2^k\right] \\ \frac{1}{1+\theta\phi}\left[(\eta_2 I_2^k + \eta_4 D_2^k)\phi + P_2^k\right] \end{pmatrix} \tag{44}$$

where

$$T_1^k = \frac{\lambda_1^k(\Lambda_1\phi + S_1^k)}{1+(\lambda_1^k+\mu)\phi},\ T_2 = 1 + \left(1 + \frac{\xi\phi}{1+k_3\phi}\right)\frac{\alpha_1(1-\tau)\phi}{1+k_2\phi},\ T_3 = \frac{\alpha_2\phi}{1+k_2\phi}\left(1 + \frac{\phi\xi}{1+k_3\phi}\right),$$

$$T_4 = \frac{\varphi\phi}{1+k_2\phi}\left(1 + \frac{\phi\xi}{1+k_3\phi}\right),\ T_5 = \frac{1}{1+k_2\phi}\left(1 + \frac{\phi\xi}{1+k_3\phi}\right),\ Z^k = \frac{\lambda_2^k(\Lambda_2\phi + S_2^k)}{1+(\lambda_2^k+\mu)\phi}.$$

The structure of the vector function G_h in (44) is so complex that we could not derive a decomposition of the type needed in Condition ($\mathcal{D}_2$). However, the factor M, with

$$\begin{aligned} M &= \max\left\{(1+k_1\phi)^{-1}, (1+k_2\phi)^{-1}, (1+k_3\phi)^{-1}, (1+k_5\phi)^{-1}, \mu(1+\mu\phi)^{-1}, \delta(1+\mu\phi)^{-1},\right. \\ &\quad \left.(1+b\phi)^{-1}, (1+\theta\phi)^{-1}\right\} \\ &< 1, \end{aligned}$$

which appears in the expression of G_h suggests that the sequence $\{Y^k\}_k$ tends to zero. We will provide in the next section numerical simulations, which show that this is the case and that the fixed-point $(X^*, 0)$ is GAS.

6 Numerical simulations

In this section, we present numerical results for the full model (6)-(7) using the nonstandard finite difference scheme (37)-(38). Unless stated differently under the figure caption, the parameters are chosen based on baseline values in Table 4. We begin by illustrating the global stability of the disease-free equilibrium as stated in Theorem 4.4 for the continuous problem, and supported by Theorem 5.4 for the corresponding nonstandard forward Euler scheme defined in Remark 5.1. In this case, with $\mathcal{R}_0 < 1$, Figure 6 shows that all trajectories converge to the disease-free equilibrium. Furthermore, for the general NSFD scheme (37)-(38), Figure 7 supports the global asymptotic stability of the disease-free equilibrium that was anticipated in Remark 5.5. Related to this, is also Figure 8 that demonstrates that the sequence, $\{Y^k\}_k$, in (44) of infected classes converges to zero.

The existence of at least one stable endemic equilibrium is emphasised in Figure 9 where we show the existence of supercritical bifurcation with respect to the basic reproduction number $\mathcal{R}_0$. Furthermore, by considering several initial conditions for $\mathcal{R}_0 > 1$, Figure 10 suggests that there exists a unique endemic equilibrium, which is globally asymptotically stable. Furthermore, in support of Theorem 4.6, we illustrate the existence of at least one Patch 1 or Patch 2 boundary equilibrium in Figure 11.

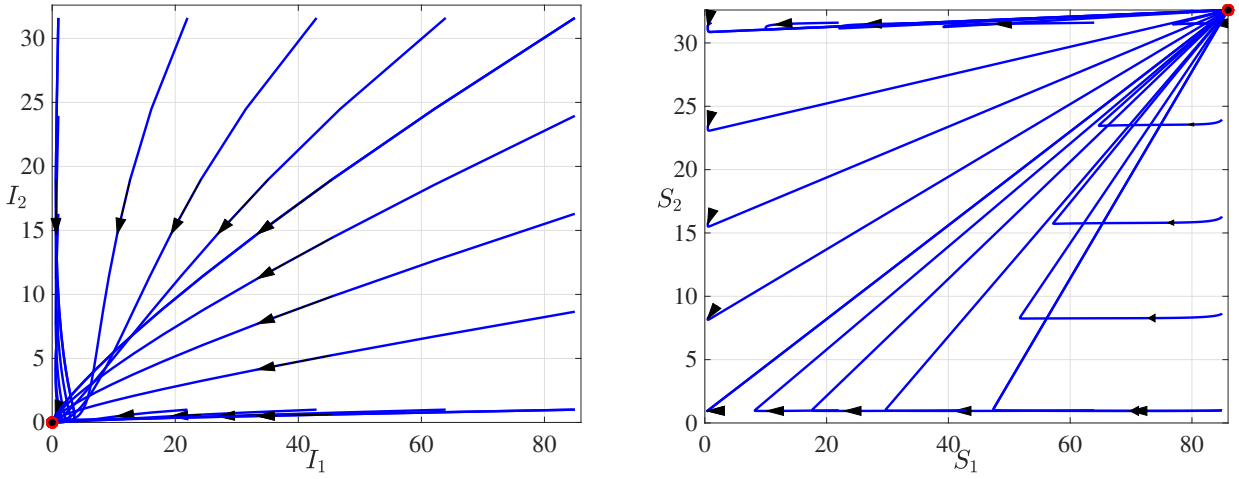

(a) (b)

Figure 6: Global asymptotic stability of the disease-free fixed point of the Nonstandard forward Euler scheme for $\mathcal{R}_0 = 0.8846 < 1$. The parameters were chosen based on baseline values with $\beta_1 = 5.041 \times 10^{-3}$, $\beta_2 = 1.340 \times 10^{-3}$, $\beta_3 = 9.518 \times 10^{-4}$, and both axes are $\times 10^6$.

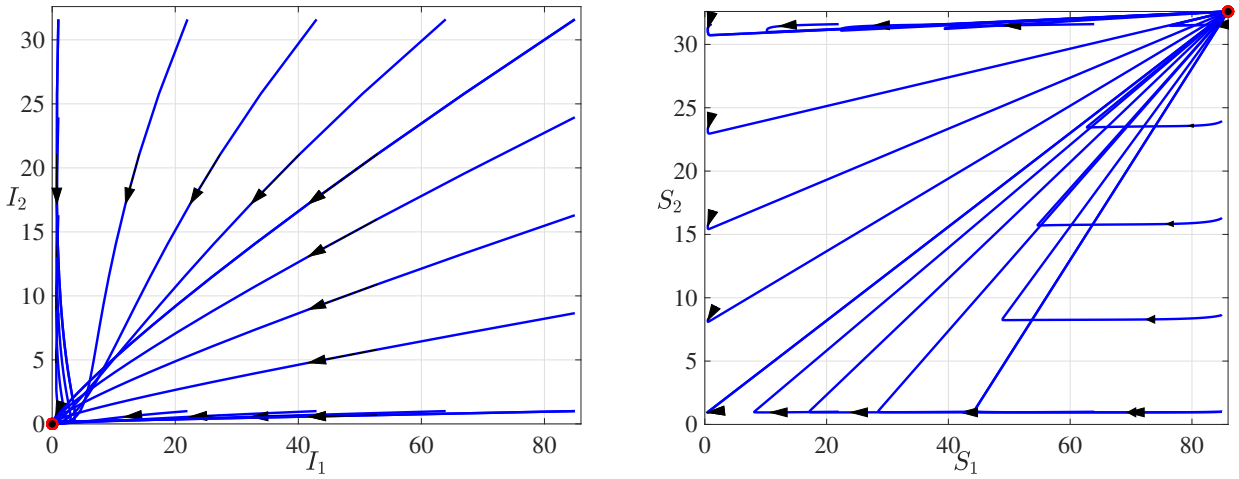

(a) (b)

Figure 7: Global stability of the disease-free equilibrium for $\mathcal{R}_0 = 0.8846 < 1$. The parameters were chosen based on baseline values with $\beta_1 = 5.041 \times 10^{-3}$, $\beta_2 = 1.340 \times 10^{-3}$, $\beta_3 = 9.518 \times 10^{-4}$, and both axes are $\times 10^6$.

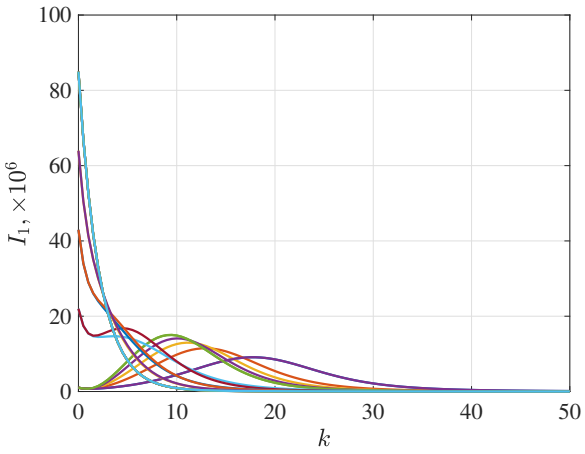

Figure 8: Illustration for the sequence of infected class, in this case I_1, defined in (44) converging to zero for different initial values.

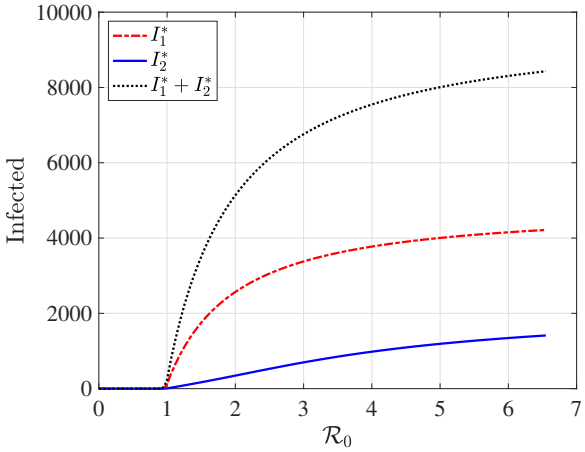

Figure 9: Supercritical bifurcation with respect to $\mathcal{R}_0$. The simulations were obtained by varying the contact rate β_2 with all other parameters fixed at baseline values.

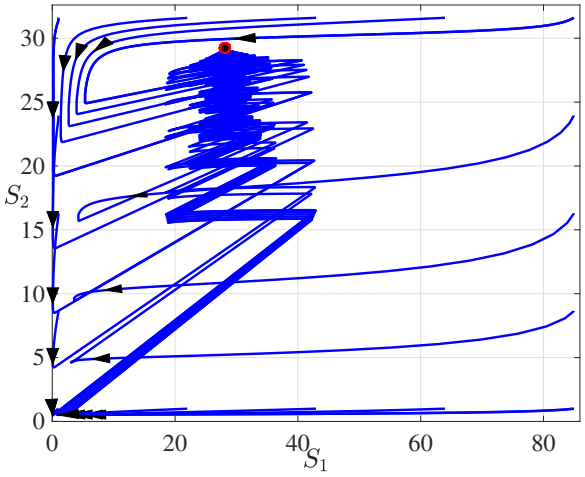

Figure 10: Asymptotic stability of the endemic equilibrium with $\mathcal{R}_0 = 2.95 > 1$, and both axes are $\times 10^6$. At the endemic equilibrium point, corresponding to the open circle, we have $I_1^* = 3254$, $D_1^* = 738$, $I_2^* = 257$ and $D_2^* = 32$.

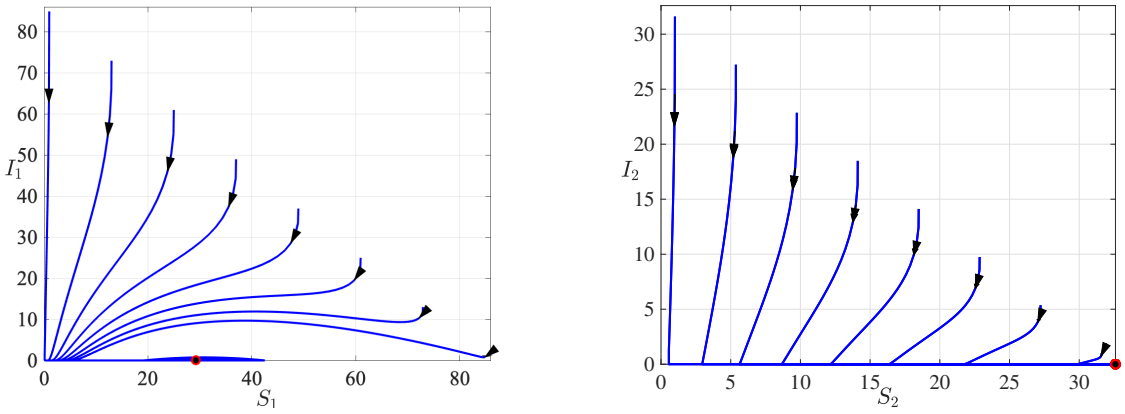

(a) (b)

Figure 11: Illustration of Theorem 4.6 on the existence and stability of the Patch 1 (a) or Patch 2 (b) boundary equilibrium with $\mathcal{R}_0 = 2.95$. The parameters were chosen based on baseline values.

Now, we come to the main focus of the work, namely the contribution of conflict/war in the transmission of EVD. We consider the severity of the epidemic and the asymptotic properties of the model with respect to conflict/war related parameters. This is assessed through simulations in Figures 12-19. First of all, Figure 12 shows the bifurcation behavior of the reproduction number $\mathcal{R}_0$ in the space (ξ, ν): one sees that, irrespective of the values of the other model parameters, having a sufficiently high number of individuals escaping the healthcare facilities, denoted by $1/\xi$, (*viz.* $\xi < 0.2$), will impede the control of Ebola when disruptive events occur, because $\mathcal{R}_0$ remains above unity. Similarly, the contour plot of $\mathcal{R}_0$ in the space (φ, τ) in Figure 13 suggests that, if all other parameters are kept as estimated/fitted in the model, except φ and τ (which can vary in their respective ranges), regardless the magnitude of destruction of healthcare facilities τ, one needs a high rate of movement of escaped individuals back into healthcare facilities (*i.e.*, $\varphi > 0.65$) for Ebola to be controlled. In Figure 14, we assess the effect of escaping individuals on the total number of infections in the population for each patch. As more individuals escape into Patch 2 from Patch 1, denoted by $1/\nu$, we see a decrease at endemic level in the total number of infections in the two populations (Figure 14(a)), *i.e.*, $\mathcal{R}_0$ increases beyond unit (Figure 12). This is supported in the Figure 14(b) where we vary the parameter ξ in the range $[0, 0.60]$ with reference to parameter range in Table 4.

The parameter τ, indicating the destruction of healthcare facilities, is one of the key measures of the impact of the conflict/war. From the flow chart in Figure 3 and the model (6)-(7), we assume that the parameters τ and α_2 are involved in the production of outflow from the I_1 and I_2 compartments such that the sums $\gamma_1 + \alpha_1(1-\tau) + \delta + \mu$ and $\gamma_2 + \alpha_2 + \delta + \mu$ are constants. While keeping the parameters γ_1, γ_2 and μ constant, we let the parameters τ and δ or α_2 and δ vary. As $\tau \to 1$ and $\alpha_2 \to 0$, the death rate δ increases. Note also that the basic reproduction number $\mathcal{R}_0 \equiv \mathcal{R}_0(\tau)$ is inversely proportional to τ. We see in Figure 15 that as the destruction parameter increases so that $\mathcal{R}_0$ decreases, the number of infected individuals in each patch increases and the number of patients in hospital, though decreasing, reach an endemic level. Note that a similar endemic state was observed in Figure 14(a) regarding increased values of the parameter ν. The dramatic impact of the destruction

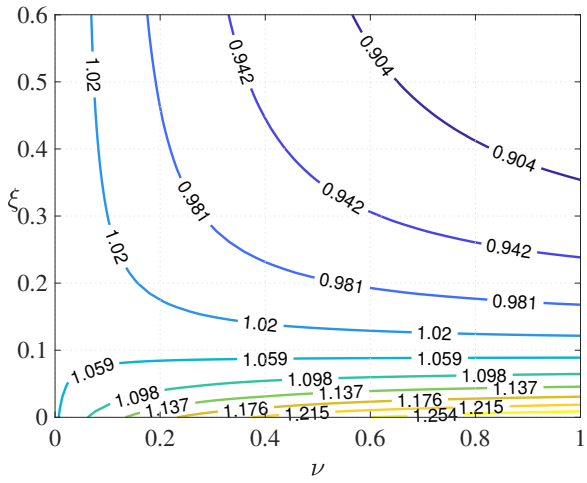

Figure 12: Contour with respect to $\mathcal{R}_0$ in the space (ξ, ν) for the model (6)-(7).

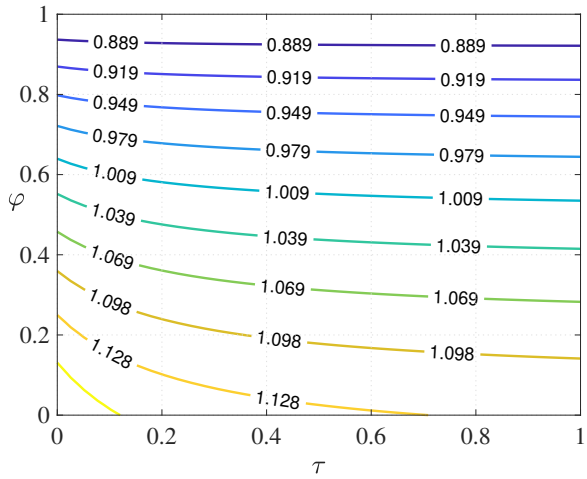

Figure 13: Contour with respect to $\mathcal{R}_0$ in the space (φ, τ) for the model (6)-(7).

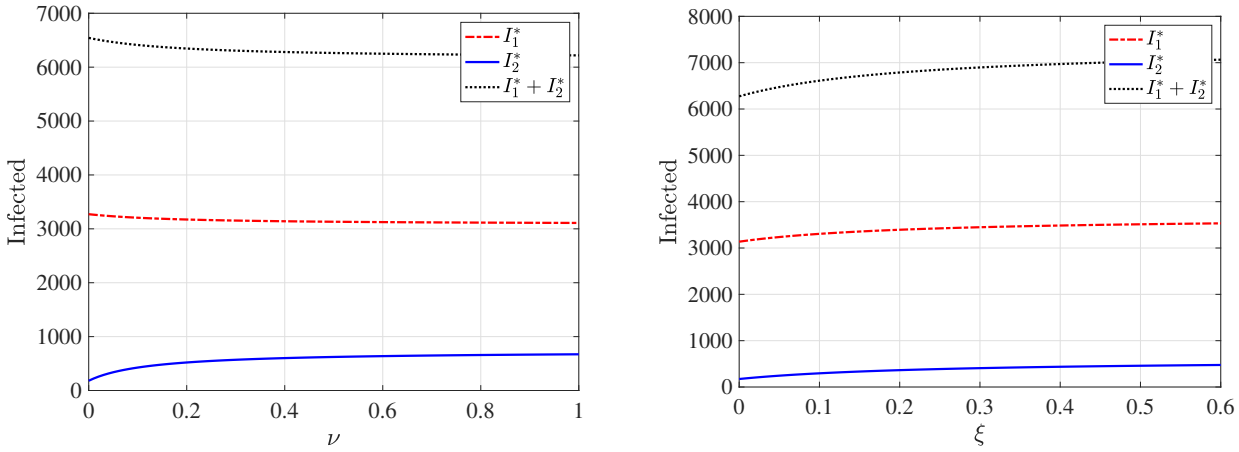

(a) Bifurcation with respect to ν. (b) Bifurcation with respect to ξ

Figure 14: Bifurcation diagram for the model (6)-(7) assessing the effect of the rate of escaping individuals moving into Patch 2, ν, and the rate of escaping from healthcare facilities, ξ.

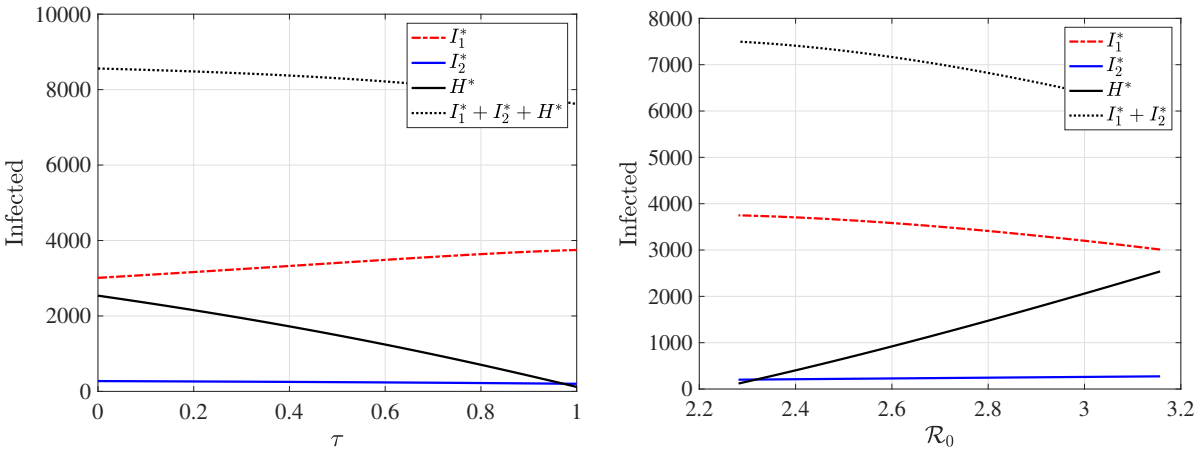

(a) Bifurcation with respect to τ. (b) Bifurcation with respect to $\mathcal{R}_0$.

Figure 15: Bifurcation diagram for the model (6)-(7) assessing the effect of the parameter of the destruction of healthcare facilities, τ, and the associated basic reproduction number, $\mathcal{R}_0$, for $b = 0.6$.

of healthcare facilities is further observed on two fronts. First, this negatively affects the behavior of people with respect to the burial of the dead and contamination of the environment. This is illustrated in Figure 16(a) for reduced values of the burial parameter b. This also is illustrated in Figure 16(b) and Figure 19(b) where η_1, η_2 and η_5 are increased. Secondly, the number of deaths is high as seen in Figure 17. This is consistent with the real data presented in Table 3.

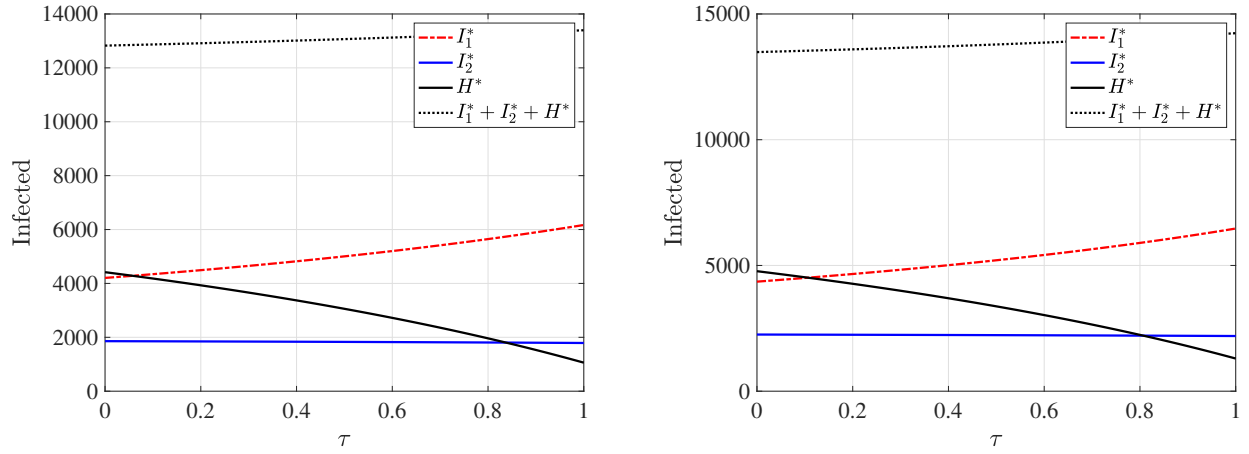

(a) $b = 0.1$. (b) $\eta_1 = \eta_2 = 2.721 \times 10^{-4}$.

Figure 16: Bifurcation diagram for the model (6)-(7) assessing the effect of the parameter of the destruction of healthcare facilities, τ.

It is generally the case that as the number of infected individuals increases, more people are sent into the health facilities for proper care. In particular, for this setup where there are no health facilities taking EVD patients in Patch 2, any identified EVD patients are sent back to Patch 1 at the rate α_2. Thus, the total number of infections decrease as $\alpha_2 \to 0$, see Figure 19(a).

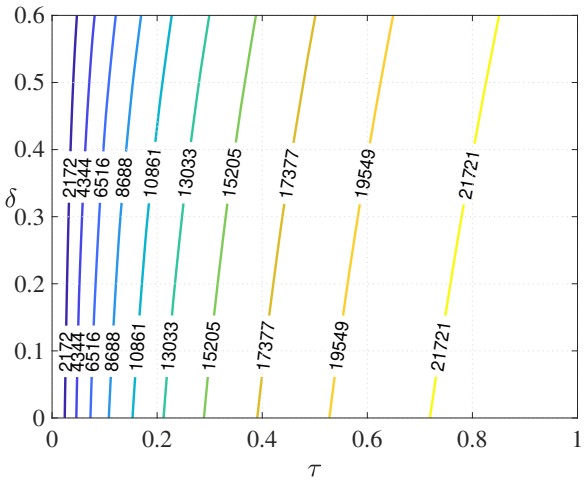

Figure 17: Contour with respect to the number of the dead for the model (6)-(7).

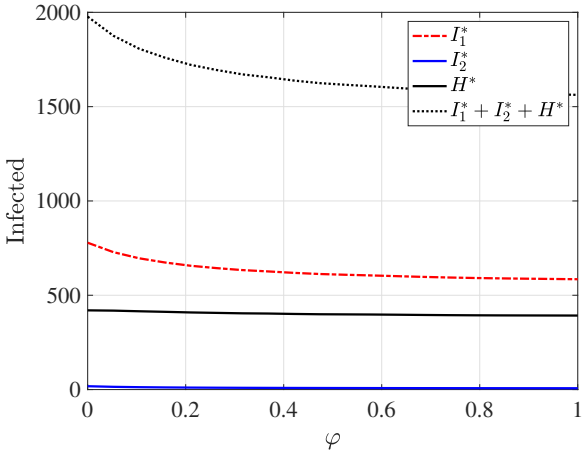

Figure 18: Bifurcation diagram for the model (6)-(7) assessing the effect of the rate of movement of escaped individuals back into healthcare facilities, φ.

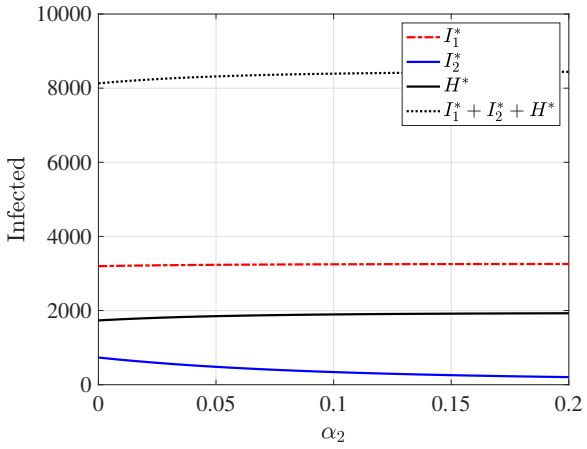

(a) Bifurcation with respect to α_2.

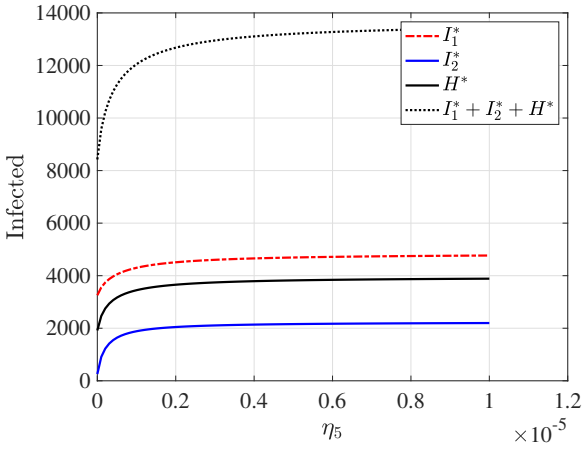

(b) Bifurcation with respect to η_5.

Figure 19: Bifurcation with respect to α_2 and η_5 to assess the effect of escaping individuals being send back to Patch 1 from Patch 2, and the effect of escaped individuals on the contamination of the environment, respectively.

7 Conclusion

Any outbreak of the Ebola Virus Disease (EVD) in Africa is on its own a major public health disaster and threat, given the associated huge numbers of deaths and the high risk of wide spread transmission to other continents (CDC 2019, WHO 2019*a*). Recently, the burden has been exacerbated by the presence of war, conflict and violence in affected regions, specifically during the tenth or 2018-2020 Ebola outbreak in the eastern region of the Democratic Republic of Congo (DRC) (WHO 2020*a*), which is the motivation and focus of this work. The war and attacks by armed groups have jeopardized interventions such as the following that made it possible to effectively and rapidly contain the previous outbreaks: role of legions of disease-fighters, educational campaign, self-protection measures, contact tracing, refrain from contaminated bush meat, vaccination, safe burial, *etc.* (Kupferschmidt 2019, Anguelov et al. 2020, Berge et al. 2017c, 2018a). In this unprecedented context of active conflict and war zone, we have investigated their impact on the transmission dynamics of the EVD.

The tenth Ebola outbreak arose precisely in a tumultuous eastern region of the DRC formed by the provinces of Ituri, North-Kivu and South-Kivu. Healthcare infrastructure and personnel constituted one of the main targets of the armed groups. This forced patients to escape from the Ebola Treatment Centers (ETCs) and to flee to the bush or neighboring provinces (referred to as Patch 2), which are war and Ebola free. In view of this setting, we constructed a two patch SIR-model. In Patch 1, consisting of the three affected provinces, we considered an extension of the classical SIR-model modified by the addition of one contaminated environment class as well as two classes of hospitalized individuals and escapees from hospitals.

Our findings are summarized as follows:

1. We carefully identified and incorporated into the model the key parameters that measure the impact of the war. These are τ, the parameter of destruction of Ebola ETCs and ξ, the rate at which patients escape from the ETCs. Furthermore, we expressed the damages caused by escaped patients in terms of two additional parameters, namely the rate ν of moving to Patch 2 and the rate η_5 of shedding the virus in the environment and bush.

2. We computed $\mathcal{R}_0$, the basic reproduction number, and established that the disease-free equilibrium (DFE) is globally asymptotically stable (GAS) whenever $\mathcal{R}_0 < 1$, while it becomes unstable when $\mathcal{R}_0 > 1$. In the latter case, we showed that the model possesses at least one Patch 1 and one Patch 2 boundary equilibria that are locally asymptotically stable (LAS). In particular, we investigated how varying the parameters τ, ξ, ν and η_5 that are embedded in the complex expression of $\mathcal{R}_0$ can contribute to reduce it below 1, or to achieve the relation $\mathcal{R}_0 > 1$, a scenario that could significantly increase the number of infectious individuals, including exporting the virus to Patch 2 and contaminating the environment.

3. Based on the recently revisited methodology in (Anguelov et al. 2020, Mickens 2020) we constructed a nonstandard finite difference (NSFD) scheme, which is dynamically consistent with respect to all the qualitative properties of the continuous model discussed in this work. In particular, we established a discrete counterpart of a decomposition result in (Castillo-Chavez et al. 2002) and used it to show that, as a discrete dynamical system, our NSFD scheme preserves

the GAS property of the DFE when $\mathcal{R}_0 < 1$.

4. In this work, there has been a great deal of real data obtained from various scientific, press and institutional sources (*e.g.* (CDC 2021, 2019, Reliefweb 2021, Wells et al. 2019, WHO 2020*a*, 2019*c*)). This enabled us to perform sound statistical data analytics that led to satisfactory parameter estimations, model-fitting and numerical simulations. In this regard, the simulations of our NSFD scheme reliably illustrated war and conflict resulting damages in terms of increased numbers of infections, as stated in items (1) and (2) above.

In (Tumutegyereize 2019), the author makes three preventive recommendations based on the experience of the West Africa Ebola outbreak from 2014-2016. These are:

- To provide clear information about Ebola and how it spreads as a strategy to downplay rumours, fuel tension and division that nurture mistrust within the community;
- To include the affected community in the planning solutions or interventions, thereby making the voices of impacted individuals heard;
- To continue supporting the Ebola affected community after the end of the outbreak.

However, since tackling Ebola in a conflict zone has proved to be difficult, complex and dangerous, one must also acknowledge that it is not easy to prevent violence with these recommendations alone, specifically in the case of an asymmetric war like in DRC where the enemy is not known. Hence, we highly recommend the following additional recommendations that enable an optimal control of the key parameters that measure the impact of war and conflict:

- Effort should be made to trace escapees and to control their movements by redirecting them to the hospitals and to the infectious class;
- Government should invest in constructing healthcare facility, particularly in regions surrounding the epicenters of the Ebola disease.
- Government should take its responsibility to protect and secure healthcare facility and personnel. Each healthcare complex should have security services, as it is the case for most public infrastructure of strategic importance in the country.
- The relevance of these recommendations is supported by our numerical simulations, which showed for instance a reduction in the total number of infections for either of the following strategies: increasing the parameter, α_2, of return from Patch 2 to Patch 1 (Figure 19(a)), reducing the destruction parameter, τ, of the hospitals (Figure 16) or increasing the rate, φ, of moving back escapees to hospitals (Figure 18).

Finally, when $\mathcal{R}_0 > 1$, our numerical simulations suggest the existence of a unique interior endemic equilibrium point, which is GAS (Figure 10). The formal proof of this fact forms an integral part of our planned future research. To this end, we intend to investigate the uniform strong persistence of this disease following the approach in (Dhirasakdanon et al. 2007). It is also our plan to investigate more complex, but realistic, models in which the challenging scenario of war and conflict is combined

with cost effective control measures such as vaccination, self-protection measures, safe burial, *etc.* (Berge et al. 2017c, 2018a), as well as the Ebanga drug against Ebola, which the United States Food Drug Administration-FDA recently approved (France24 2021).

Acknowledgements:

The authors acknowledge the support of the South African DSI-NRF SARChI Chair in Mathematical Models and Methods in Bioengineering and Biosciences. MC & JL acknowledge the support, in part, of the DSI-NRF Centre of Excellence in Mathematical and Statistical Sciences (CoE-MaSS), South Africa. The authors are grateful to the anonymous reviewers, the Editor-in-Chief and the Handling Editor for their excellent suggestions and comments that have greatly contributed to improve the manuscript.

References

Agusto, F. B., Teboh-Ewungkem, M. I. & Gumel, A. B. (2015), 'Mathematical assessment of the effect of traditional beliefs and customs on the transmission dynamics of the 2014 ebola outbreaks', *BMC Medicine* **13**(1), 1–17.

Anguelov, R., Berge, T., Chapwanya, M., Djoko, J. K., Kama, P., Lubuma, J. M.-S. & Terefe, Y. (2020), 'Nonstandard finite difference method revisited and application to the Ebola virus disease transmission dynamics', *Journal of Difference Equations and Applications* **26**(6), 818–854.

Anguelov, R., Dumont, Y., Lubuma, J. M.-S. & Shillor, M. (2014), 'Dynamically consistent nonstandard finite difference schemes for epidemiological models', *Journal of Computational and Applied Mathematics* **255**, 161–182.

Anguelov, R. & Lubuma, J. M.-S. (2001), 'Contributions to the mathematics of the nonstandard finite difference method and applications', *Numerical Methods for Partial Differential Equations: An International Journal* **17**(5), 518–543.

Bani-Yaghoub, M., Gautam, R., Shuai, Z., Van Den Driessche, P. & Ivanek, R. (2012), 'Reproduction numbers for infections with free-living pathogens growing in the environment', *Journal of Biological Dynamics* **6**(2), 923–940.

BBC News (2018), 'DR Congo election: Protesters attack Ebola centre in Beni, 27 December 2018', (Protesters). Last accessed on September 12, 2021.

Berge, T., Chapwanya, M., , Lubuma, J. M.-S. & Terefe, Y. A. (2018a), 'A mathematical model for Ebola epidemic with self-protection measures', *Journal of Biological Systems* **26**(01), 107–131.

Berge, T., Lubuma, J. M.-S., Moremedi, G. M., Morris, N. & Kondera-Shava, R. (2017c), 'A simple mathematical model for Ebola in Africa', *Journal of Biological Dynamics* **11**(1), 42–74.

Bibby, K., Casson, L. W., Stachler, E. & Haas, C. N. (2015), 'Ebola virus persistence in the environment: state of the knowledge and research needs', *Environmental Science & Technology Letters* **2**(1), 2–6.

Bichara, D. & Iggidr, A. (2018), 'Multi-patch and multi-group epidemic models: a new framework', *Journal of Mathematical Biology* **77**, 10–134.

Buseh, A. G., Stevens, P. E., Bromberg, M. & Kelber, S. T. (2015), 'The Ebola epidemic in West Africa: Challenges, opportunities, and policy priority areas', *Nursing Outlook* **63**(1), 30–40.

Busenberg, S. & Cooke, K. (2012), *Vertically transmitted diseases: models and dynamics*, Vol. 23, Springer Science & Business Media.

Castillo-Chavez, C., Feng, Z. & Huang, W. (2002), On the computation of $\mathcal{R}_0$ and its role on global stability, *in* 'Castillo-Chavez C, van den Driessche P, Kirschner D, Yakubu A, eds. Mathematical Approaches for Emerging and Reemerging Infectious Diseases: An Introduction', Vol. 126, Springer Science & Business Media.

Castillo-Chavez, C. & Song, B. (2004), 'Dynamical models of tuberculosis and their applications', *Mathematical Biosciences & Engineering* **1**(2), 361.

CDC (2019), '2014-2016 Ebola outbreak in West Africa', (West Africa). Online; accessed 10 September 2021.

CDC (2021), 'Ebola virus disease distribution map: Cases of Ebola Virus Disease in Africa since 1976', (Map). Online; accessed 10 September 2021.

Dhirasakdanon, T., Thieme, H. R. & van Den Driessche, P. (2007), 'A sharp threshold for disease persistence in host metapopulations', *Journal of Biological Dynamics* **1**, 363–378.

Diekmann, O. & Heesterbeek, J. A. P. (2000), *Mathematical epidemiology of infectious diseases: model building, analysis and interpretation*, Vol. 5, John Wiley & Sons.

DRC Ministry (2021), 'Direction surveillance epidémiologique, (ministère de la santé publique de la republique démocratique du Congo, rapport annuel (2020) de surveillance des maladies prioritiaires en republique démocratique du Congo'.

France24 (2021), 'Ebola epidemic: Ebanga treatment arrives on market after FDA approval', (Ebanga Drug). Online: Accessed 17 September 2021.

Goldstein, T., Belaganahalli, M. N., Syaluha, E. K., Lukusa, J.-P. K., Greig, D. J., Anthony, S. J., Tremeau-Bravard, A., Thakkar, R., Caciula, A., Mishra, N. et al. (2020), 'Spillover of Ebolaviruses into people in eastern Democratic Republic of Congo prior to the 2018 Ebola virus disease outbreak', *One Health Outlook* **2**(1), 1–10.

Iggidr, A., Sallet, G. & Tsanou, B. (2012), 'Global stability analysis of a metapopulation SIS epidemic model', *Mathematical Population Studies* **19**(3), 115–129.

Kasereka, M. C., Sawatzky, J. & Hawkes, M. T. (2019), 'Ebola epidemic in war-torn Democratic Republic of Congo, 2018: Acceptability and patient satisfaction of the recombinant vesicular stomatitis virus–Zaire Ebolavirus vaccine', *Vaccine* **37**(16), 2174–2178.

Kraemer, M. U., Pigott, D. M., Hill, S. C., Vanderslott, S., Reiner, R. C., Stasse, S., Brownstein, J. S., Gutierrez, B., Dennig, F., Hay, S. I. et al. (2020), 'Dynamics of conflict during the Ebola outbreak in the Democratic Republic of the Congo 2018–2019', *BMC Medicine* **18**(1), 1–10.

Kruk, M. E., Rockers, P. C., Williams, E. H., Varpilah, S. T., Macauley, R., Saydee, G. & Galea, S. (2010), 'Availability of essential health services in post-conflict Liberia', *Bulletin of the World Health Organization* **88**, 527–534.

Kupferschmidt, K. (2019), 'Ebola veteran promises an end to Congo's epidemic', *Science* **365**, 526–527.

La Salle, J. P. (1976), *The stability of dynamical systems*, SIAM, Philadelphia, Pennsylvania.

Legrand, J., Grais, R. F., Boelle, P.-Y., Valleron, A.-J. & Flahault, A. (2007), 'Understanding the dynamics of Ebola epidemics', *Epidemiology & Infection* **135**(4), 610–621.

Maxmen, A. (2018), 'War zone complicates roll-out of ebola vaccine in latest outbreak', *Nature* **560**(7718), 289–289.

Maxmen, A. (2019), 'The Ebola Wars: the World Health Organization is battling bullets, politics and deadly disease in one of the world's most troubling outbreaks', *Nature: Feature News* **573**, 178–182.

McPake, B., Witter, S., Ssali, S., Wurie, H., Namakula, J. & Ssengooba, F. (2015), 'Ebola in the context of conflict affected states and health systems: case studies of Northern Uganda and Sierra Leone', *Conflict and Health* **9**(1), 1–9.

Médecins Sans Frontières (2021*a*), 'DRC's tenth Ebola outbreak', (10^{th}). Online: accessed 5 March 2021.

Médecins Sans Frontières (2021*b*), 'Ebola outbreak in Democratic Republic of Congo: community engagement is vital to an effective response', (Community Engagement). Online: accessed 5 March 2021.

Médecins Sans Frontières (2021*c*), 'Twelfth outbreak declared in North Kivu province: Crisis Update', (12^{th}). Online: accessed 5 March 2021.

Mickens, R. E. (1994), *Nonstandard finite difference models of differential equations*, World Scientific, Singapore.

Mickens, R. E. (2020), *Nonstandard Finite Difference Schemes: Methodology and Applications*, World Scientific, Singapore.

Omondi, T. & Sheriff, I. D. M. A. (2010), 'Sierra Leone's long recovery from the scars of war', *Bulletin of the World Health Organization* **88**, 725–726.

Piercy, T., Smither, S., Steward, J., Eastaugh, L. & Lever, M. (2010), 'The survival of filoviruses in liquids, on solid substrates and in a dynamic aerosol', *Journal of Applied Microbiology* **109**(5), 1531–1539.

Reliefweb (2019), 'DR Congo: Attacks on ebola response, July-August 2019', (Attacks-1). Online: accessed 10 September 2019.

Reliefweb (2021), 'DR Congo: Attacks on healthcare during the 10th ebola response in the Democratic Republic of the Congo', (Attacks-2). Online: accessed 10 September 2021.

Richardson, J. S., Dekker, J. D., Croyle, M. A. & Kobinger, G. P. (2010), 'Recent advances in ebolavirus vaccine development', *Human Vaccines* **6**(6), 439–449.

Shuai, Z., Heesterbeek, J. & van Den Driessche, P. (2013), 'Extending the type reproduction number to infectious disease control targeting contacts between types', *Journal of Mathematical Biology* **67**(5), 1067–1082.

Shuai, Z. & Van den Driessche, P. (2015), 'Modelling and control of cholera on networks with a common water source', *Journal of Biological Dynamics* **9**(1), 90–103.

Siewe, N., Lenhart, S. & Yakubu, A.-A. (2020), 'Ebola outbreaks and international travel restrictions: Case studies of Central and West Africa regions', *Journal of Biological Systems* **28**(02), 431–452.

Stuart, A. & Humphries, A. R. (1998), *Dynamical systems and numerical analysis*, Vol. 2, Cambridge University Press, Cambridge.

Tsanou, B., Bowong, S. & Lubuma, J. M.-S. (2017a), 'Global stability of a two-patch cholera model with fast and slow transmissions', *Mathematics and Computers in Simulation* **133**, 142–164.

Tsanou, B., Bowong, S., Lubuma, J. M.-S. & Mbang, J. (2017b), 'Assessing the impact of the environmental contamination on the transmission of ebola virus disease (EVD)', *Journal of Applied Mathematics and Computing* **55**(1), 205–243.

Tumutegyereize, K. (2019), 'What lessons can we learn from West Africa about preventing violence in the Democratic Republic of Congo during the Ebola outbreak? Conciliation Resources: Peace building during an Ebola crisis', (Lessons). Online: accessed 10 September 2021.

Van den Driessche, P. & Watmough, J. (2002), 'Reproduction numbers and sub-threshold endemic equilibria for compartmental models of disease transmission', *Mathematical Biosciences* **180**(1-2), 29–48.

Van den Driessche, P. & Watmough, J. (2008), Further notes on the basic reproduction number, *in* 'Brauer F., van der Driessche P. and Wu J. (eds), Mathematical epidemiology: Lecture Notes in Mathematical Biosciences Subseries', Vol. 1945, Springer, pp. 159–178.

Walter, W. (2012), *Differential and integral inequalities*, Vol. 55, Springer Science & Business Media.

Wells, C. R., Pandey, A., Mbah, M. L. N., Gaüzère, B.-A., Malvy, D., Singer, B. H. & Galvani, A. P. (2019), 'The exacerbation of ebola outbreaks by conflict in the Democratic Republic of the Congo', *Proceedings of the National Academy of Sciences* **116**(48), 24366–24372.

WHO (2014), 'Ebola virus disease fact sheet no. 103', (Fact sheet). Last accessed on 2015 Jan 11.

WHO (2017), 'Ebola virus disease, Democratic Republic of Congo: External Situation Report 22 (2017)', (WHO Report 22). World Health Organization Report.

WHO (2019*a*), 'Ebola outbreak in the Democratic Republic of the Congo declared a public health emergency of international concern', (PHEIC). World Health Organization Report.

WHO (2019*b*), 'Ebola virus disease Democratic Republic of Congo: External Situation Report 50', (Report-50). World Health Organization Report.

WHO (2019*c*), 'Ebola virus disease, Democratic Republic of Congo: External Situation Reports 08, 11, 14 & 21 (2018) and 25, 34, 38, 43, 47, 52, 56, 60, 65, 69, 73 & 78 (2019)', (WHO reports archive). World Health Organization Report.

WHO (2020*a*), 'Ebola outbreak 2018-2020 North Kivu/Ituri, DRC', (Kivu-Ituri). World Health Organization Report.

WHO (2020*b*), 'Ebola virus disease Democratic Republic of Congo: Emergencies Preparedness, Response: Disease outbreak news: Update, 2 January 2020', (Fact sheet). World Health Organization Report.

WHO (2020*c*), 'Ebola virus disease Democratic Republic of Congo: External Situation Report 98', (Report-98). World Health Organization Report.

World Bank (2017), 'Physicians (per 1,000 people) - Sub-Saharan Africa', (Physicians). Online: accessed 10 September 2021.

World Bank (2019*a*), 'Birth/death rate, crude (per 1,000 people) - Congo, Dem. Rep.', (Birth-Death). Online: accessed 10 September 2021.

World Bank (2019*b*), 'Hospital beds per 1000 people', (Hospitals). Online: accessed 10 September 2021.

World Bank (2019*c*), 'Population density (people per sq. km of land area) - Congo, Dem. Rep.', (Population Density). Online: accessed 18 March 2022.